2008

Resonance ultrasonic vibrations and photoluminescence mapping for crack detection in crystalline silicon wafers and solar cells

Andrii Monastyrskyi
University of South Florida

Resonance Ultrasonic Vibrations and Photoluminescence Mapping for Crack Detection in Crystalline Silicon Wafers and Solar Cells

by

Andrii Monastyrskyi

A thesis submitted in partial fulfillment
of the requirements for the degree of
Master of Science in Chemical Engineering
Department of Chemical and Biomedical Engineering
College of Engineering
University of South Florida

Co-Major Professor: John Wolan, Ph.D.
Co-Major Professor: Sergei Ostapenko, Ph.D.
Scott Campbell, Ph.D.

Date of Approval:
October 1, 2008

Keywords: renewable energy, photovoltaic, cracks detection, acoustic, standard deviation

Acknowledgements

First of all I would like to thank my major professor Dr. Sergei Ostapenko for his help, technical guidance and expertise, patience during my research work that led to this Master, and for all other support that I have received.

I would also like to thank Dr. John Wolan, who was of great help and shared his expertise with me while motivating me to work and study harder and obtain better results.

And last but certainly not least, I would like to thank Dr. Igor Tarasov, who had had the patience to help me in many aspects of resonance ultrasonic vibrations area as well as photoluminescence segment of this work.

Table of Contents

List of Tables

List of Figures

Resonance Ultrasonic Vibrations and Photoluminescence Mapping
for Crack Detection in Crystalline Silicon Wafers and Solar Cells

Andrii Monastyrskyi

ABSTRACT

The solar energy, or photovoltaic (PV) industry, driven by economic competition with traditional fossil energy sources, strives to produce solar panels of the highest conversion efficiency and best reliability at the lowest production cost. Solar cells based on crystalline silicon are currently the dominant commercial PV technology by a large margin, and they are likely to remain dominant for at least one decade. The problem of improvement mechanical stability of silicon wafers and finished solar cell is one of the most critical for entire PV industry. Mechanical defects in wafer and cells in the form of periphery or internal cracks can be initiated at various steps of the manufacturing process and becomes the trigger for the fracture. There are a limited number of characterization methods for crack detection but only a few of those are able to satisfy PV industry needs in sensitivity of the crack detection incorporated with the analysis time. The most promising are a Resonance Ultrasonic Vibrations (RUV) technique and Photoluminescence (PL) imaging.

The RUV method was further developed in this thesis project for fast non-destructive crack detection in full-size silicon wafers and solar cells. The RUV methodology relies on deviations of the resonance frequency response curve measured on a wafer with peripheral or bulk millimeter-length crack when it is compared with identical non-cracked wafers. It was observed that statistical variations of the RUV

parameters on a similarly processed silicon wafers/cells with the same geometry lead to false positive events reducing accuracy of the RUV method. A new statistical approach using three independent RUV crack detection criteria was developed and applied to resolve this issue. This approach was validated experimentally. Crack detection using RUV technique was applied to a set of production-grade Cz-Si wafers and finished solar cells from the Isofoton's S.A. (Spain) production line. Cracked solar cells rejected by the RUV method using the statistical approach were imaged with room temperature PL mapping and independently controlled with Scanning Acoustic Microscopy (SAM). A comparison of three independent techniques for crack detection, RUV, PL and SAM, was performed on selected samples. A high accuracy and selectivity of the RUV method to identify mm-size cracks in wafers and cells was confirmed.

Chapter 1: Introduction and Background

1.1 Defining the necessity for renewable sources of energy

The fossil energy is non-renewable source of energy as it takes millions of years to form. The defining feature of global energy markets remains high in 2007 and unsteady prices reflecting a tight balance of supply and demand [1]. World energy consumption is projected to expand by fifty percent from 2005 to 2030 in the International Energy Outlook 2008 reference case projection [2]. Although high prices for oil and natural gas, which are expected to continue throughout the period, are likely to slow the growth of energy demand in the long term, world energy consumption is projected to continue increasing violently as a result of strong economic growth and enlarging populations in the world's developing countries. The complete revision of the world fossil sources of energy usage has to be initiated. This already has put issues such as energy security, energy trade and alternative energies at the forefront of the political agenda worldwide. Environment issues linked closely with the move towards a more sustainable development path are leading the drive to develop and deploy cleaner technologies.

Renewable energy technologies are well placed to contribute to improving environmental concerns. Over the past five years renewable energy prices have fallen to a

point where most are now cost competitive with fossil technologies when all values (environment, jobs, security, etc.) are considered. The present cost of renewable sources of energy is affordable for certain markets but it is still too high to actually compete with conventional energy sources. This leaves space for further research and development. The energy of sun, wind and water has to be used as the level of the world energy consumption is constantly high. Electricity is the most versatile form of energy we have and as long as light is shining on the solar cell it generates electrical power which helps decrease our dependence on conventional energy sources.

1.2 Silicon for photovoltaic cells

Photovoltaic (PV) cells are devices that convert directly sunlight into electricity bypassing thermodynamic cycles and mechanical generators. Cells are packaged in photovoltaic modules which are electrically connected making solar photovoltaic arrays. PV production has been doubling every two years, increasing by an average of 48 percent each year since 2002, making it the world's fastest-growing energy technology [2]. At the end of 2007, global solar cell production was 7,911 megawatts.

At present the vast majority of photovoltaic cells are made from silicon. Crystalline silicon in a form of single crystal, polycrystalline or ribbon wafers, was responsible for almost 90% of worldwide PV production in 2001. The conversion efficiency for single-silicon commercial modules ranges between 18-20%. Currently the average price for single-crystal modules is $2.5 - 3.8 per peak watt. The energy conversion efficiency for a commercial module made of polycrystalline silicon ranges

between 14 to 16% with average price of $3.91 per peak watt. Single-silicon modules are also very reliable for outdoor power applications. The wafering in which ingots are cut into less than 200 μm wafers is most expensive and time-consuming stages. It is clear that resulting wafers are very fragile.

Despite of dominant position of single silicon on PV market, it was recognized that other semiconductors could make good solar cells. Most of them exist in a form thin semiconductor layer of PV materials that is deposited on a low-cost supporting layer such as glass, metal or plastic foil. Thin film solar cells can be expected to provide cost reduction and energy savings in cell manufacture. Of the large variety of solar cell types investigated, the most popular are gallium arsenide [GaAs], cadmium telluride [CdTe], and copper-indium-diselenide [$CuInGaSe_2$]. Copper Indium Diselenide thin-film materials have the highest energy conversion efficiency of up to 18% (in individual cells), but its complexity makes it manufacturing more complicated.

1.2.1 Mono-crystalline silicon

Manufacture of the mono-crystalline silicon solar cells is an outgrowth of the methods used for microprocessors fabrication. A major difference is a high purity of row polysilicon which is critical for electronic device manufacturing and is less important for PV cell production. Although various techniques have been utilized to grow single crystals of silicon, two techniques have dominated in the production of silicone single crystals: Czochralski method and Float-Zone method.

The Czochralski (CZ) method is the most common method of growing single

crystal ingots. The seed crystal is lowered in molten silicon doped with a p-type impurity such as boron and drawn upward under tightly controlled conditions of temperature, and linear and rotational speed [3].

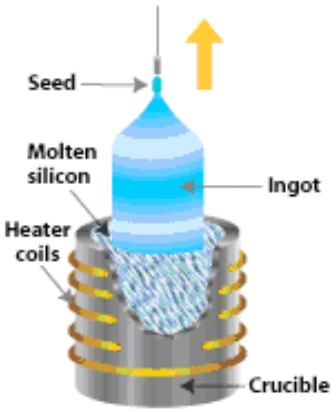

Figure 1.1 Czochralski method of silicon growth [4].

Manufacture of the mono-crystalline silicon solar cells is an outgrowth of the methods used for microprocessors fabrication. A major difference is the purity of silicon which is critical for electronic device manufacturing and is not needed for PV cells production. Therefore the major source for silicon solar cell production is the waste material from the microelectronics device fabrication.

CZ method produces cylindrical ingots of typically 100-200 mm diameter, although ingots of the largest silicon ingots produced today are 400 mm in diameter and 1 to 2 meters in length. PV silicon wafers with approximately 0.2 mm thickness are then cut from the initial ingots. While silicon is grown by the CZ method, the melt is contained in a quartz crucible and the contamination by oxygen in the silicon ingot from the walls of the silica should not exceed 10^{18} atoms per cm^3 [5]. Sensitive to oxygen

impurity accessories must be developed using other crystal growth methods [6].

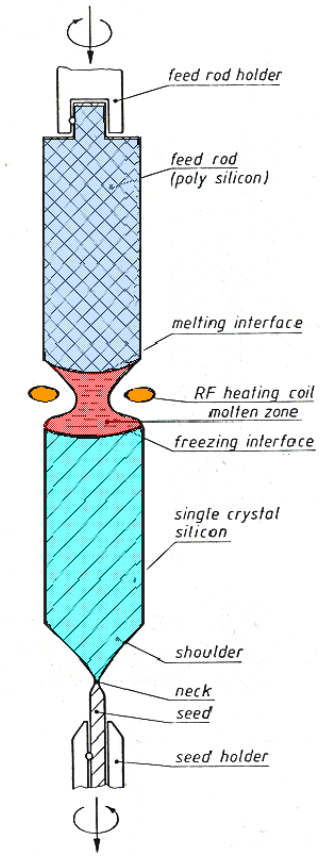

Figure 1.2 Float-Zone method of silicon crystalline growth [9].

The Float-Zone (FZ) method is originated from zone melting which was used to refine binary alloys and was invented by Theuerer [8]. The first FZ crystal was grown by Keck and Golay in 1953 [7]. In the FZ method a polysilicon rod is converted into a single crystal ingot by passing a molten zone from one end of the rod to the other. The ingot is moved linearly and rotationally under controlled conditions and a high-purity, low oxygen containing single crystal could be formed with the help of the seed crystal. The

dimensions of FZ wafers are generally less than 150mm due to the surface tension limitations during growth.

The molten silicon does not contact any substances other then ambient gas in the growth chamber and FZ crystal contains less then 10^{16} atoms of oxygen per cm^3. Inherently then FZ crystal is distinguished by its higher purity and resistivity [8]. Nowadays FZ silicon is employed for premium high-efficiency cell applications and CZ Si is used for higher-volume, lower-cost applications.

1.2.2 Polycrystalline silicon

Polycrystalline silicon (poly-Si) wafers are capable of producing cells of about 80% of the performance of cells built on a single crystalline wafer. Today, 50% of the world's supply of polysilicon is being used for production of solar power panel . The poly-Si wafer has higher packing density due to rectangular geometry which makes poly-Si PV modules competitive on the market. The polycrystalline silicon wafers are also less fragile and can be cut into one-third the thickness of CZ material.

The starting material for high purity poly-Si is silica. The melting and reduction of silica gives metallurgical grade silicon (MG-Si) with purity about 98-99%. However, to be useful as a semiconductor material in solar cells, silicon must be refined to a purity of 99.99%. Thus the next step is to purify MG-Si to the level of semiconductor grade purity. The basic concept is that powdered MG-Si is reacted with anhydrous HCl to form various chlorosilane compounds in a fluidized-bed reactor. Then the silanes are purified by distillation and chemical vapor deposition (CVD) to form semiconductor-grade silicon

[8].

There are several methods of producing poly-Si wafers but most accepted are sheet or ribbon silicon growth and direct ingot casting. In the casting process, molten silicon is directly cast into a mold and allowed to solidify into an ingot. In order to overcome surface stress within parallel aligned carbon molds it uses a centrifugal casting approach. The cooling rate is one factor that determines the final size of crystals in the ingot and the distribution of impurities. Despite initially promising results this approach is no longer used widely [40].

The second commercially developed is ribbon growth approach which is modification of the Edge-defined Film-fed Growth (EFG) technique. This method involves pulling of silicon ribbon to heights of up to 6 m from the graphite dies with the source of molten silicon. A frame holds the thin sheet of material when pulled from the melt. In the EFG method the ribbon is pulled in the form of a polygon (8 or 12 facets) in which the sides could be cut by a laser to individual wafers (12.5 × 12.5 cm2) [40, 41].

In 1997, Evergreen Solar Inc developed and commercialized string ribbon technology which implies use of two high temperature resistant strings drawn in the melted silicon. The pulling of silicon to about 7-8 mm is allowing the crystallization which becomes the ribbon. In this case, temperature control at liquid-solid phase is less demanding in comparison to the EFG method [40].

Despite the fact of lower manufacturing cost of poly-Si, it is offset by the lower cell efficiency.

1.2.3 Amorphous silicon

Amorphous silicon (α-Si) is another allotropic form of the silicon with noncrystalline structure. Atoms are not arranged in any particular order in α-Si and they contain large numbers of structural and bonding defects. In 1974 amorphous silicon began to be used in photovoltaic devices by properly controlling the conditions under which it was deposited and by carefully modifying its composition, for example, by plasma enhanced chemical vapor deposition (PECVD).

In the current production method for α-Si solar cells, individual layers are deposited in a high frequency glow discharge reactor. Hydrogen and silicon are split from the mixture of silane (SiH_4) and hydrogen [11]. The α-Si can then be transferred onto metal or glass. The addition of diborane (B_2H_6,) or phosphine (PH_3) are used for appropriate p and n doping [12].

Thin film can absorb 90% of the usable solar energy because for a given layer thickness amorphous silicon absorbs solar radiation 40 times more efficiently than single-crystal silicon does. This is one of the most important factors affecting its potential for low cost. Other principal economic advantages are that amorphous silicon can be produced at a lower temperature and can be deposited on low-cost substrates. These characteristics make amorphous silicon the leading thin-film PV material.

Despite achieved efficiency of 13% (low defect density deposition technique and use of anti-reflection films) the critical problem of α-Si solar cells is their stability. Weak silicon-hydrogen bonds tend to be broken in the amorphous material due to the recombination of light generated charge particles. This degradation was first researched

by Staebler and Wronski and the effect was named after them [13].

Today, amorphous silicon is commonly used for solar-powered consumer devices that have low power requirements – calculators, watches.

1.3 Fracture and cleavage in silicon

One of the major current technological problems for the PV industry is to identify and eliminate potential sources of mechanical defects such as microcracks leading to the loss of wafer integrity and ultimate breakage of processed silicon wafers and finished solar cells [35].

Generally speaking fracture occurs when the energy available for crack enlargement is sufficient to overcome the resistance of the material. Hooke's law of elasticity states that the amount by which a material body is deformed (the strain) is linearly related to the force causing the deformation (the stress). There are two different approaches to fracture analysis: the energy criterion and the stress intensity approach. Griffith and Irwin found an expression for the constant *G* in terms of the surface energy of the crack [14]:

$$\mathcal{G} = \frac{\pi \sigma_f^2 a}{E} \qquad \text{equation 1.3.1}$$

where σ_f, is the fracture stress, *E*, is the Young's modulus, and a, is the crack area. In the moment of fracture critical energy release rate *G* is a measure of fracture toughness. Silicon fracture has been studied extensively for the last few decades and is

reported to have two principal cleavage planes: (111) and (110) [15-17]. The lowest fracture energy at which a crack propagated in (111) plane is 2.2 J/m2 which is twice the surface energy density. The energy needed for fracture of already defected silicon material is even lower [16]. Fracture can be characterized by crack direction [15], propagation speed [16], and also the atomistic mechanisms of fracture [17].

Wafer breakage during PV processing is a very high cost issue. Propagation of cracked cells into the end modules would cause failure of the end unit. Downtime of several minutes caused by wafer failing and cleaning of scattered parts is not acceptable at a high-throughput production level typically a few seconds per wafer. Additional stress at the process step of already cracked wafers causes crack elongation followed by wafer breakage. Electrical failures during cell and module tests is also common. It was shown that cracks in readily processed solar cells lead to a weak recombination current. Cracks are also causing serious ohmic shunts especially if wafer has it before processing or screen-printing the contact metallization [35]. The shunts described above may also emerge if there are any holes presented in a cell, e.g., resulting from laser cutting [18].

1.4 Crack detection methods

Currently mono- as well as poly-crystalline Si wafers are sliced thinner with thicknesses down to 150 microns in order to reduce production costs and compensate for the feedstock shortage. Wafers having a high level of residual elastic stresses behave extremely unpredictably during processing and handling. Usually cracks are introduced at the sawing stage of blocks/ingots. Those cracked wafers processed as normal and even

more cracks are added during the later stages such as solar cell processing. About 0.5% undetected defective cells end up in modules which makes approximately 74,000 defective cells per year with yearly loss close to $1M.

To improve the economics of cell manufacturing, the PV industry requires a development of specialized inspection and quality control tools for integration into the production process. Dallas in 2006 [39] identify that this in-line tool should allow (1) rejection of mechanically unstable Si wafers after ingot slicing before wafers are introduced into further cell processing, (2) identification of wafers with mechanical defects (such as cracks) during production to avoid their in-line breakage, (3) detection of cracked cells before they will be laminated into modules to avoid panel efficiency reduction and product return from the field. The testing tool must possess the following features at a minimum: (i) high speed data acquisition and analysis, matching the approximately 2 seconds per wafer throughput rate of typical cell lines; (ii) high stability (reliability and duty cycle) of the hardware performance including wafer loading/unloading and parts movement; (iii) easy integration into a belt conveyor configuration or cell testing station, an (iv) user-friendly algorithm for wafer/cell rejection with a minimum number of false positives. There are numbers of experimental results published for crack detection in Si wafers and a majority of them have been based on imaging techniques. The most interesting are optical and ultrasonic methods such as, optical transmission [19], photoluminescence [21] and electro-luminescence imaging [23], infrared lock-in ultrasound thermography [25], impact testing [30], and scanning acoustic microscopy [26, 27].

In Table 1.1 we compared different methods for crack inspection currently under

investigation and prototyping.

An alternative new approach for stress control and crack detection in solar grade Si wafers and cells using the Resonance Ultrasonic Vibrations (RUV) system was developed by a research group at the University of South Florida [33].

Table 1.1 Comparison of crack detection methods

Method	Strength	Weakness
Scanning Acoustic Microscopy	High spatial resolution, 10 microns	Wafer must be immersed in water, Long data acquisition time above 10 minutes per whole wafer ;
IR thermography	High spatial resolution (below 1 mm), imaging technique	Long acquisition time to use for in-line control (> 1 minute per wafer)
Luminescence	High throughput, snap-shot imaging	Interference with other defects (scratches, dislocations) , Closed cracks are hidden due to diffraction limit.
Optical transmission	High throughput, high sensitivity	Not applicable in case of closed cracks and final cells with back contacts
Impact testing	High throughput	Minimum crack length is above 25 mm
Resonance Ultrasonic Vibrations (RUV)	High throughput (<2.0 seconds per wafer); Applicable for in-line control; No interference with scratches and other defects	Sensitivity to crack length is limited by wafer statistics; Do not identify crack location, only “reject-accept” protocol (basic model)

1.4.1 Optical transmission

The optical μ-crack detection method was developed at the beginning of the century at the University of Konstanz, Germany and is said to be viable as an inspection

tool for inline characterization of wafers and finished cells with throughput rates of up to 2.500cells/hr [19,20]. In this method the silicon wafer is placed above a broad spectrum flash-light with an intensity of approximately 1000 suns. A high resolution CCD camera is used to detect the optical transmission through the wafer (Figure 1.3).

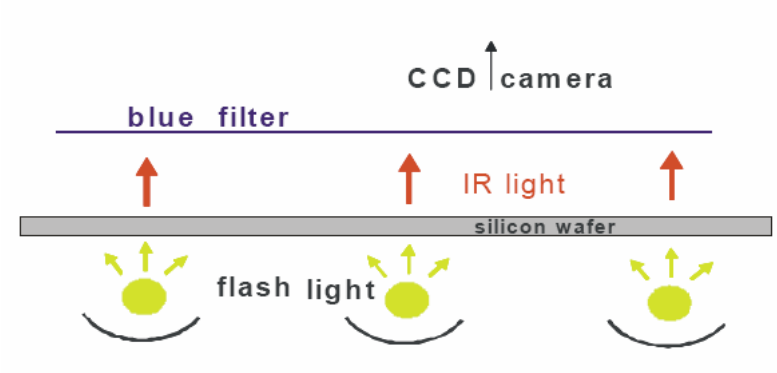

Figure 1.3 Optical transmission µ-crack detection apparatus [19].

Individual wafer thickness and crystal structure affect the infrared portion of the light passes through the sample. CCD camera is detecting those modulation and can detect 1-5 µM cracks while for cracks smaller than 1 µM infrared detection system is sufficient (Figure 1.4).

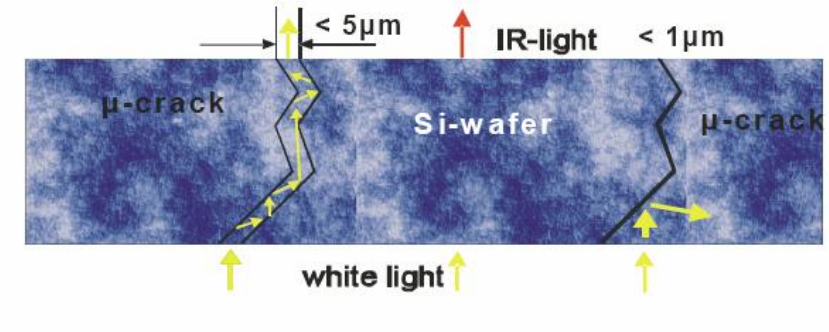

Figure 1.4 Diagram of µ-crack widths and detection mechanism [19].

However, small peripheral wafer cracks would not be visible using optical transmission. Also due to the optical diffraction limit, closed cracks within the wafer's surface with 1 µm width would not be detectable. Complete solar cells and wafers having backside aluminum contact are also not suitable for crack detection using this technique due to metal interference.

1.4.2 Photoluminescence and electroluminescence imaging

Luminescence is a process in which light is emitted from a material at different wavelengths after external energy was delivered and absorbed. Luminescence is somewhat opposite to basic PV operation where photon energy exceeding a certain band gap energy, is applied to a valence electron, causing the bonds to brake and the electron to move to the conduction band. Various types of luminescence are identified which differ by a source of external energy, such as photoluminescence (external light), electroluminescence (electric field), cathodoluminescence (electron beam), etc.

Photoluminescence (PL) is a process in which a chemical compound absorbs a photon with a wavelength in the range of visible or UV electromagnetic radiation, thus transitioning to a higher electronic energy state, and then radiates a photon back out, returning to a lower energy state. The period between absorption and emission is typically extremely short, on the order of 10 nanoseconds [3].

Trupke et al [21, 22] used photoluminescence imaging to view process defects in silicon wafers. In order to get PL image, a 15 W /815 nm diode laser was used to illuminate the sample. Lifetime distribution can then be analyzed within an area of

interest. PL signal was detected using a cooled CCD one mega pixel camera with a 1000 nm longpass filter located between the sample and CCD camera to prevent incident laser light from contributing to the measured PL intensity. Thus PL is contactless and can be applied to monitoring silicon wafers carrier lifetime at different stages of production. Authors also reported data acquisition time of 1.5 s and spatial resolution of 130 μm.

The minority carrier diffusion length distribution could also be analyzed using electroluminescence imaging [23]. Electroluminescence (EL) is a form of luminescence which is the result of radioactive electron-hole recombination in semiconductor material. The excited electrons then release their energy as light (photon). Fuyuki et al [23] had found that the intensity distribution of light emission agreed with the mapping of minority carrier diffusion length in silicon active layers. Emitted from the silicon wafer infrared light was collected by the cooled CCD camera in the 300–1100 nm region. Emission intensity increased linearly with the diffusion length. The spatial resolution was 250 μm (Figure 1.5).

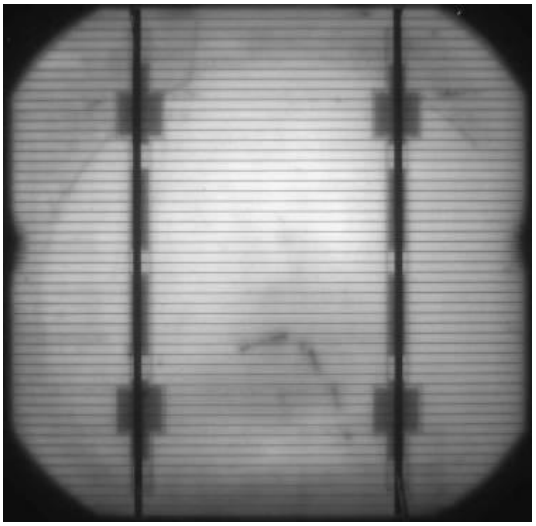

Figure 1.5 EL images of an industrial screen printed solar cell [23].

Both PL as EL techniques are fast and contactless but are lacking the capability of identification and differentiation between actual crack and surface scratch which will be shown later.

1.4.3 Infrared lock-in ultrasound thermography

Rakotoniaina et al [25] had employed the Ultrasound lock-in thermography (ULT) method for detection of cracks in silicon wafers and solar cells not long ago. The principle of crack detection by ULT is based on the heat created by the cracks flanks because of their friction caused by the ultrasound driven into the silicon wafer. The special resolution of the method depends on the quality of IR camera incorporated into the ULT setup. Their lock-in thermography system allowed imaging of periodic surface temperature modulations at frequencies up to 54 Hz having an effective value as low as 10 mK using 1/2 hour measure time. This long acquisition time is required for signal averaging due to low infrared intensity and makes ULT unsuitable for in-line crack detection where no more than a couple of seconds are accepted for quality control. Also optically invisible cracks could be detected, etched cracks do not lead to local heat sources and might require covering the wafer surface with black paint which considerably enhances the IR signal.

1.4.4 Scanning acoustic microscopy

The use of ultrasound methods had been established in industry in the early 1900s. The acoustic waves with frequency over 20 kHz are referred as ultrasonic waves, meaning above the upper level limit of human's hearing. Ultrasound techniques are used widely in military and medicine. For example medical sonography – nondestructive diagnostic medical imaging technique used to visualize muscles, tendons, and internal organs, their size, structure and any pathological lesions is purely based on acoustic phenomena.

Lemons and Quate developed the first scanning acoustic microscope (SAM) in 1974 at Stanford University [27]. But before that the C-scan was used as a nondestructive testing (NDT) method since the 1950s. Modern SAMs are the hybrid tools with characteristics of both the first Stanford's SAM and the C-scan. SAM was used by the IC industry extensively for a long time, although the PV manufacturers began to employ acoustic microscopy technique for crack detection in silicon wafers and solar modules for a relatively short time [26].

SAM is a pulse-echo microscope that operates a focused transducer which generates and receives the ultrasonic pulses reflected beneath the front surface of the sample [29]. The piezoelectric crystal acts as active element in the transducer which generates an ultrasonic impulse. Concave lens are attached to the tip of the transducer. Image visualization is produced by passing the transducer across the sample. Scan time varies from seconds to minutes depending on the desired resolution and the area of scan. The coalescence of longitudinal and flexural waves interference is reflected from the

surface and from the back side of the surface. The reflection contrast is patterned when separate layers within a structure isolated using time separation. Ultrasonic waves are very sensitive to the density variations (such as voids or air gaps) so a coupling medium is required. Immersion tank is normally employed to run most of the inspections. SAM is a non-destructive package analysis when imaging the internal features of the sample.

The area of distortion is identified as acoustic impendence discontinuity at damaged silicon wafer or cell. Acoustic impedance is a ratio of the acoustic pressure to the particle velocity per unit area [29] and can be expressed as:

$$Z_i = \rho_i * v_i \qquad \text{Equation 1.4.4.1}$$

where Z_i is an acoustic impedance of the material in the *i*-th layer, ρ_i is a density of the material in the *i*-th layer, and v_i = velocity of sound in the *i*-th layer. The magnitude and time of travel of the reflected signal provide crucial information about the material.

SAM has proven to be an accurate method for identifying cracks and microcracks in wafers and partially processed solar cells. It can provide information about where cracks and microcracks are occurring and be a useful tool in quantitative analysis of those (Figure 1.6)

However, each SAM wafer measurement took 20 minutes for sample set-up and data collection. This is clearly not an in-line production process. The data from this effort was very useful as the sample set evaluated by SAM can now be used to calibrate and verify the accuracy of any new methods developed for crack detection.

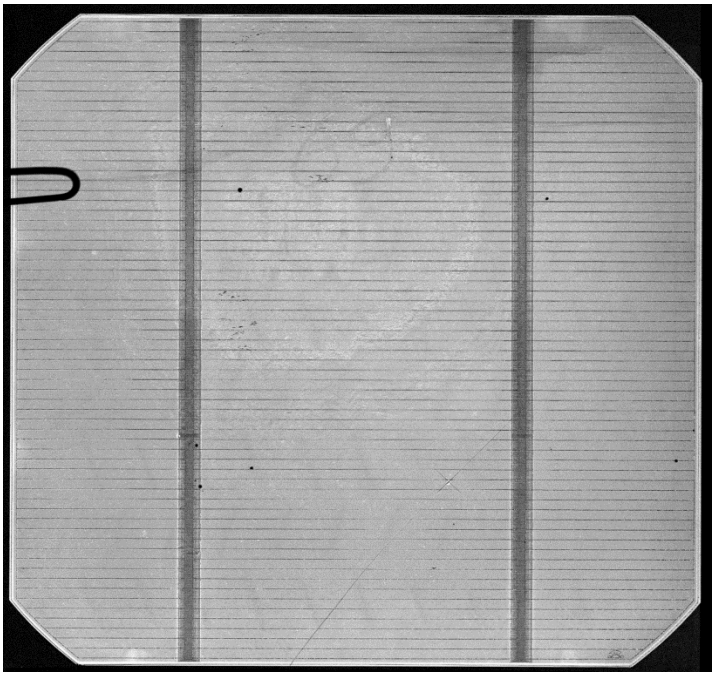

Figure 1.6 SAM image of solar cell sample showing a crack along
the periphery. Image sizes 160mm x 160mm, crack length is about 100 mm total.

1.4.5 Impact testing

Recently Hess's research group at USF reported new technique for crack detection in silicon wafers [30]. In this method the audible response in the frequency range up to 2,000 Hz after a mechanical impact on a Si wafer is analyzed. In the experiment setup, a piezoelectric hammer with a vinyl tip applies the mechanical impact to the silicon wafer which is placed on a piece of convoluted foam. The microphone is mounted 2 cm above the wafer picking up the impact response and is allowed to calculate the frequency response with the impact force defined as the input and the sound pressure

level as the output.

A picture showing the impact testing apparatus is shown in Figure 1.7.

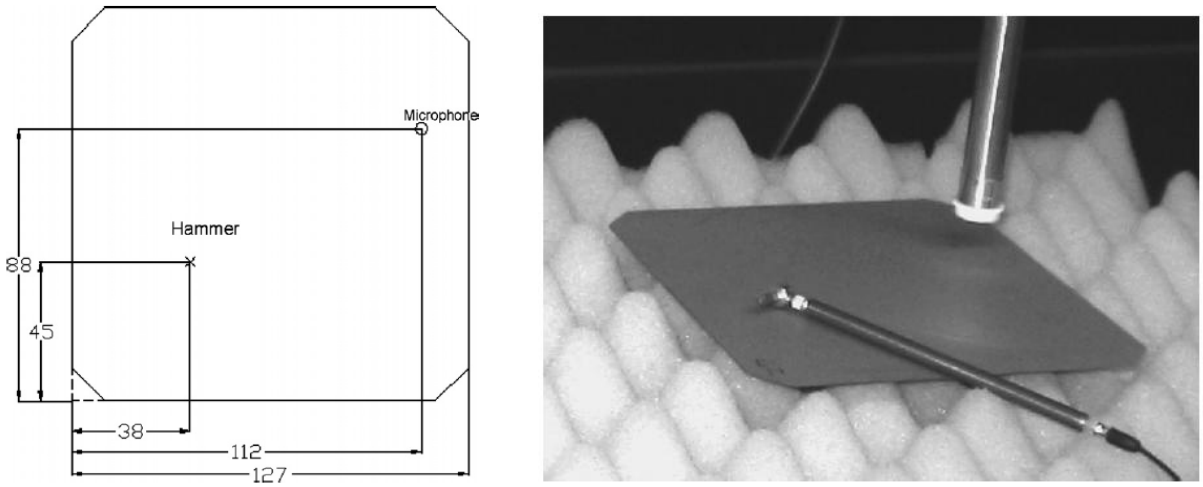

Figure 1.7 Impact testing apparatus including impact hammer, wafer, and microphone [30, 31].

Cracked wafers showed a decrease in natural frequency, a decrease in peak magnitude, and a larger bandwidth which corresponded to crack response from the RUV technique [32]. Peak amplitude has been found to be most sensitive to the cracked wafers. Impact testing allows identification of cracks with total length of 10 mm only.

1.5 Resonance ultrasonic vibrations

The Resonance Ultrasonic Vibrations (RUV) is a technique for non-destructive stress control and crack detection in full-size silicon wafers and solar cells [33, 35]. In a case of crack detection, the RUV methodology relies on deviation of the resonance frequency response curve of a wafer with peripheral or bulk millimeter-length crack

versus regular non-cracked wafers. Three RUV frequency curve crack rejection criteria were proposed: (1) shift of the peak position downward; (2) increase of the bandwidth, and (3) reduction of the amplitude.

1.5.1 Development of the RUV system

The RUV as a method of detecting deficient wafers was developed at USF in 2002 [32, 33]. This technique involves exciting entire silicon wafer with tunable frequency and recording the response from it at defined regions. The deviation of the frequency response curve of a wafer with a periphery crack versus undamaged wafers is analyzed.

The wafer is positioned on the transducer which is connected to the vacuum pump through the cross section in the center of the transducer (Figure 1.8). Once the wafer is placed on the proper size base the transducer goes up on the moving Z stage triggering the vacuum pump to turn on which creates small negative pressure from the back side. This pressure (about 50 kPa) keeps the wafer in a specific location and allows the transducer to induce resonance vibrations in the form of standing waves into the sample. A transducer frequency can be swept in the ultrasonic range from 20 kHz to 100 kHz using a function generator (WaveTec 10 MHz DDS 29) [31-34] and amplified by a power amplifier (Samson Servo 260). Ultrasonic vibrations are propagated into the wafer and detected using a high sensitive broadband ultrasonic probe at the edge of the wafer.

Figure 1.8 3-D image of the piezoelectric transducer with cross-hatching for vacuum contact, positioned beneath a sample wafer.

Thin layer of chemical mechanical planarization (CMP) pad material is attached to the probe active side in order to control applied force. The vibrations are then fed into the lock-in amplifier (Stanford Research Systems SR-850) [42].

The Lock-in amplifier is used to detect a very small AC signals from the probe and separate it from the noise (Figure 1.9). It detects signal based on modulation at some known frequency. A reference frequency is essential for the measurement as lock-in encounters the response from the frequency sweep and separates components of the signal at a specific reference frequency and phase using phase-sensitive detection technique. Noise signals, at frequencies other than the reference frequency, are cancelled out and do not affect the measurement.

The accurate positions of the wafer, transducer and the probe are regulated by

stepper motors. The whole RUV system is PC controlled and operated by Windows-based original software.

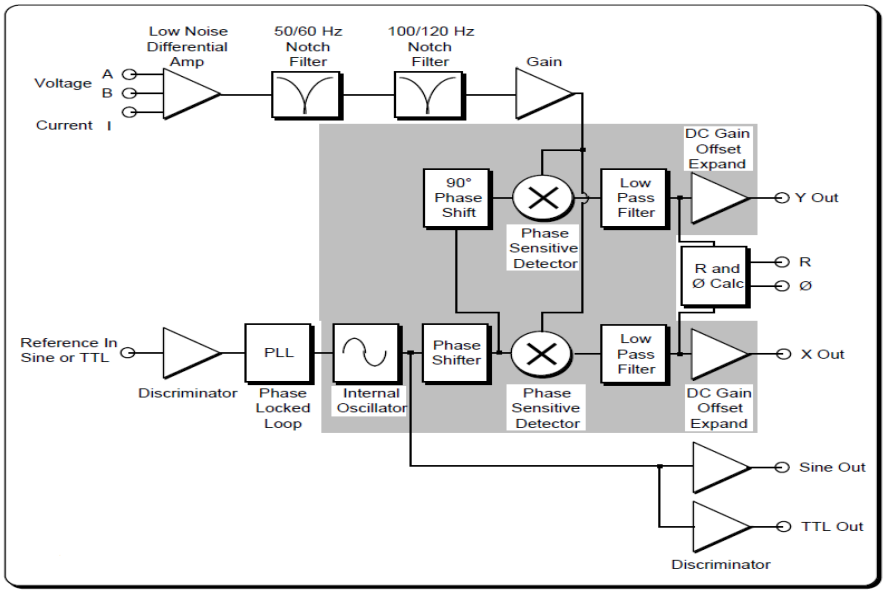

Figure 1.9 SR850 Lock-In functional block diagram [42].

The RUV measures single resonance curve and then analyzes each of the rejections parameters of defected wafer in comparison to undamaged one. Each silicon wafer however differs in physical properties such as size, weight, and thickness. This alteration induces changes in peak position, peak bandwidth, and peak amplitude and small variations of these parameters are acceptable. However it also might provoke a generation of false positive events when undamaged wafer is recognized as a potentially cracked one.

RUV technique is also not capable of providing information of exact location of the crack.

1.5.2 Current system description

The current model of RUV system (RUV-2) provides a controlled delivery of the ultrasonic vibrations in the form of a frequency sweep into a solar-grade silicon (Si) wafer or solar cell using external ultrasonic transducer. High sensitive ultrasonic probe measures the resonance ultrasonic vibrations of the wafer at a specific frequency range, which depends on the wafer size and shape. Resonance vibrations generated by the wafer provide a sensitive feed-back on mechanical quality of the wafer or solar cell. Frequency scans identify the wafer mechanical problems such as stress or cracks.

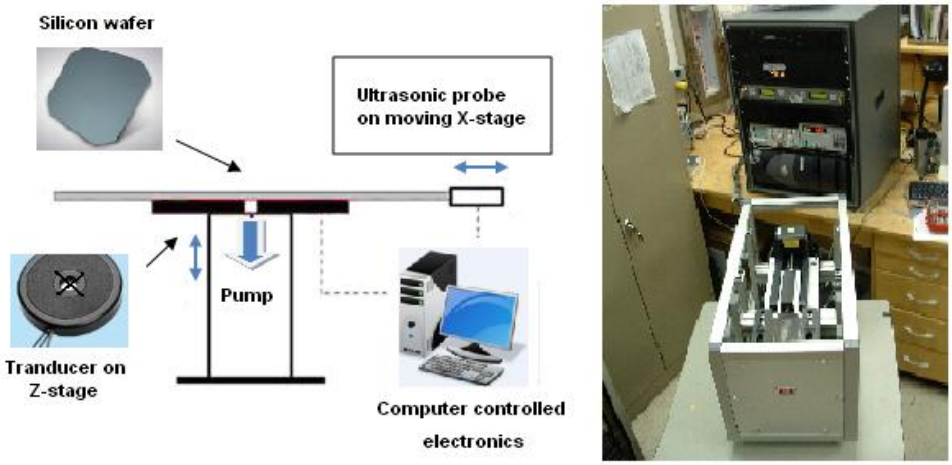

Figure 1.10 A basic schematic of the experimental RUV system.

The RUV-2 (basic version) is composed of two parts (Figure 1.10): (a) measuring unit, which include the X and Z moving stages with ultrasonic transducer and ultrasonic probe; and (b) computer controlled electronics, including PC with Windows-based software (Figure 1.12). The measuring unit is a place where the measurements occur. The

unit consists of a broad band ultrasonic transducer located on a moving Z-stage, the ultrasonic probe (high frequency microphone) attached to the moving X-stage, and a wafer holder. The stages are controlled by rack mounted electronics comprised of (a) lock-in amplifier; (b) stepping motor controller; (c) power amplifier, (d) DC power supply, (e) oscilloscope, and (f) vacuum pump [31, 35].

The computer with GPIB interface card and original software operates the RUV-2 system. Built-in function generator in Stanford SR-850 lock-in amplifier is used to generate the frequency sweep. The signal from the probe is directly fed to the lock-in without amplifying which significantly reduces acquisition time.

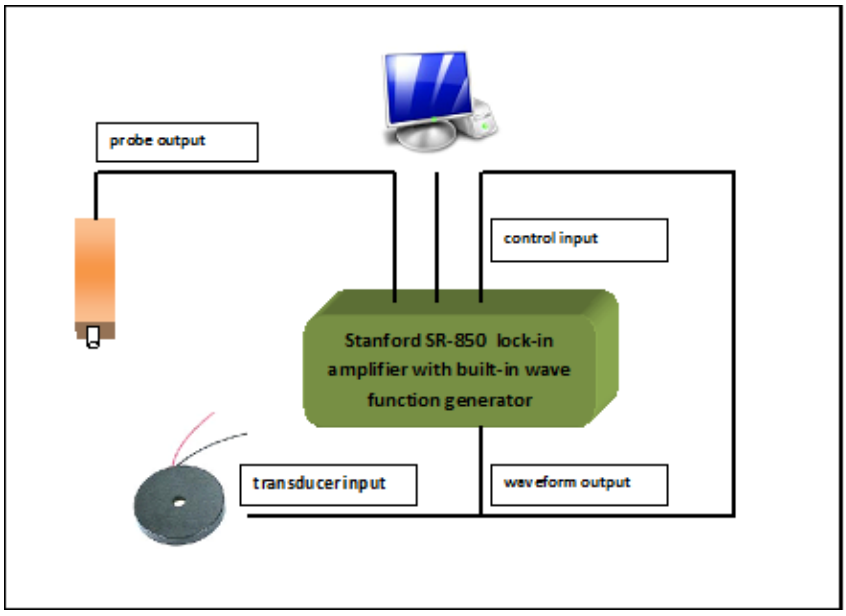

Figure 1.11 An electrical schematic of the RUV system.

The RUV-2 system is also a PC controlled unit with Windows-based software providing system operation, data acquisition and data processing.

The RUV user interface id shown in Figure 1.12 .

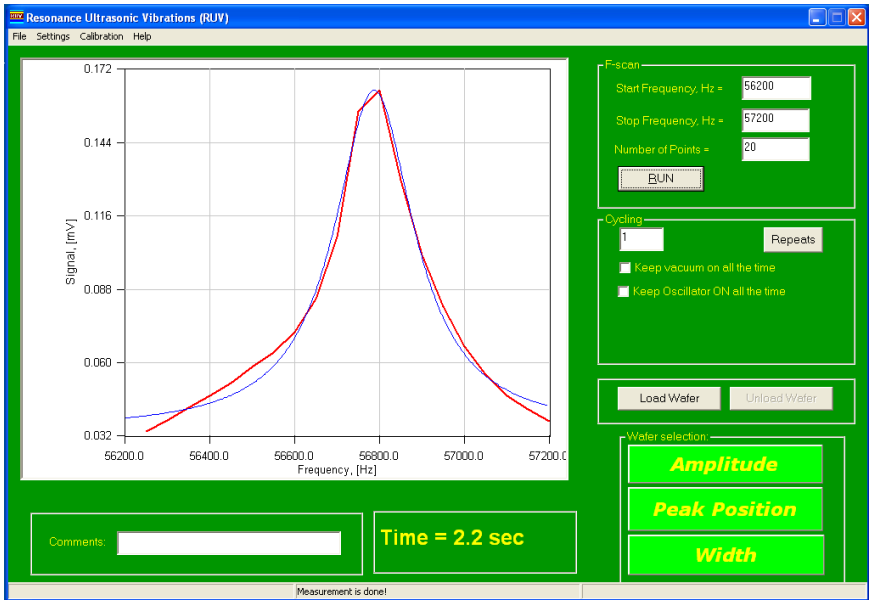

Figure 1.12 RUV program user interface screen shot.

By pressing ‘RUN’ button the measuring cycle starts. The transducer on Z-stage moves up and picks up the wafer, vacuum switch opens and applies negative pressure between the wafer and transducer, the probe located on the X-stage moves toward the wafer and contacts the wafer’s edge allowing ~ 1mm spring displacement. F-scan runs and displays in the window (Figure 1.12). The row f-scan data can be saved in the ‘File-Save Raw Data’ menu. Vacuum sensor measures and displays the value of negative pressure in mm Hg.

A principal RUV peak is approximated by a Lorentzian curve. Parameters of the approximation (amplitude, peak position and band width) are stored in the selected data file. Consecutive repeated measurements add new approximation parameters to the data

file. At the end of the multiple runs the data can be exported to Microsoft Excel in the File menu for statistical evaluation.

The RUV-2 system also allows performing a calibration for follow-up crack detection using calibrated set of wafers. In the calibration protocol RUV-2 system finds statistical parameters of the normal or σ-distribution (average value and standard deviation) on a calibrated set of similar wafers/cells which are measured sequentially. These statistical parameters for resonance peak amplitude, bandwidth and peak position are saved. The parameters are used to quickly identify wafers/cells with f-scan characteristics different from average values by 1- σ, 2- σ or 3- σ (selected in sub-menu).

The duration of the measuring cycle can be varied by changing the number of data points per f-scan or lock-in amplifier integration time. In Figure 1.13, the frequency sweeps performed with different data points per f-scan (from 100 to 10) and cycling time from 12.4 seconds down to 2.0 seconds per cycle. Throughput rate of 2 seconds is an achievable rate for the RUV-2 system. Reduction of the data points per scan provides only a small variation of the f-scan parameters.

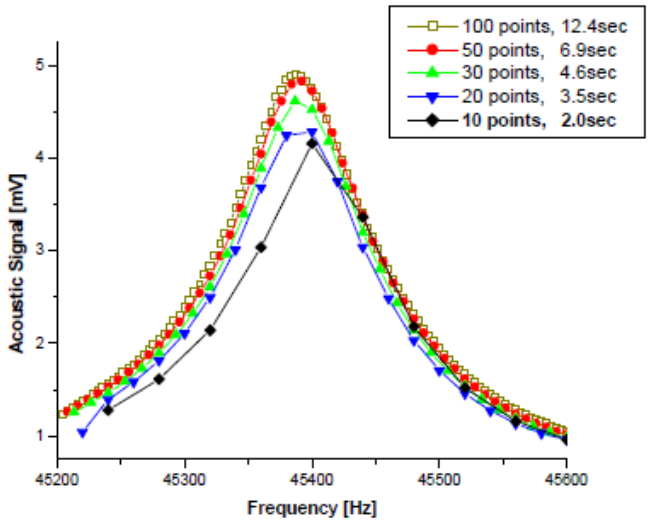

Figure 1.13 RUV parameter shift due to decreasing number of points.

This allows RUV-2 prototype unit be integrated into an automatic belt-moving solar cell production line or used as a stand-alone testing system for quality control.

Chapter 2: Experiments

2.1 RUV system setup

In Figure 1.9 a schematic of the RUV system with details published elsewhere [31, 35] is shown. RUV-2 system was used for all experiments as described above. The entire RUV measurement cycle consisted of the consecutive steps: wafer loading from a home position on the transducer by vacuum-coupling the wafer and transducer, lifting the transducer with the wafer to a measuring position using computer-controlled Z-stage, contacting the wafer's edge by ultrasonic probe using computer-controlled X-stage, data acquisition by measuring f-scan, Lorentzian fit of the experimental data, and wafer unloading to the home position.

Data stored in .txt files then was analyzed using scientific graphing and data analysis software Origin 6.0.

2.2 PL system setup

AlGaAs laser diode (pulsed) with emission wavelength at 804 nm and maximum output power 150 mW in pulse (model Spectra Diode Labs, SDL 800) was used as the excitation sources in the PL experiments. The photoluminescence signal was dispersed

with a 0.5 m SPEX-500M grating spectrometer possessing a reciprocal dispersion of 3.2 nm/mm (2nd order) with a 600 lines/mm diffraction grating. The dispersed signal was registered with a liquid nitrogen cooled Ge detector (North Coast Scientific Corp.) in the range of 1050 – 1550 nm. AC signal from the detectors was fed to Lock-in amplifier EG&G Model 5209 and collected by a computer. The PL mapping experiment was done with the use of an X-Y computer controlled moving stage (Velmex 8300) with 10 μm step precision. All PL experiments were performed at room temperature. A schematic of the PL setup for PL measurement is shown on Figure 2.1.

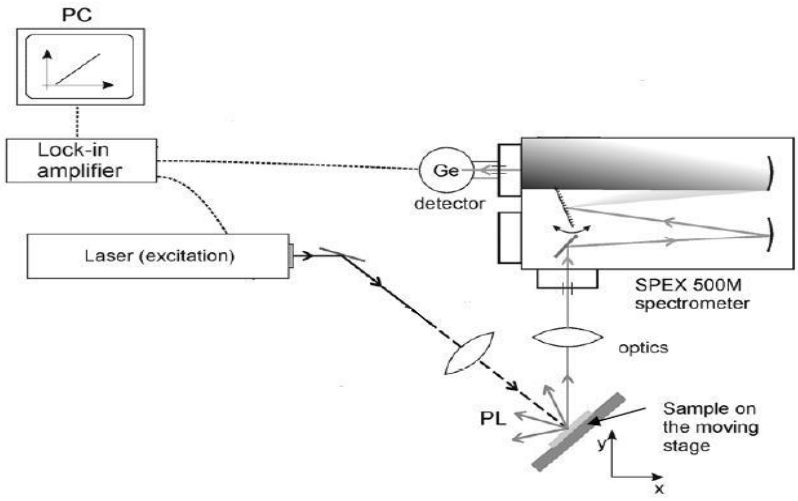

Figure 2.1 Photoluminescence setup for room temp measurements of Si wafers and cells

2.3 SAM system setup

SONIX HS1000 HiSPEED™ by Sonix, Inc. was used for all SAM experiments. The emitting transducer of SONIX also serves as the receiving transducer upon reflection of the ultrasound pulses (DPR002S digital broad band pulser/receiver with emitting frequency up to 150 MHz). The general setup of HS1000 is shown on Figure 2.2. The instrument is also equipped with 1 µM encoder for enhanced resolution. Silicon wafer or cell is emerged into the coupling media which is DI water. Step motors (SMD1000C) then are allowing to map pulse magnitude in transverse plane by moving the stage with a transducer [29]. The speed and scan area can be controlled by WinIC Lab™ original software version 3.5.1. The cracks as small as 10 µM can be identified and located using SAM technique. The reflection from back surface only analyzed. The resolution of 100 µM was sufficient to visualize such a damaged wafer. The average time for scanning 158x158 mm wafer/cell is 24 minutes.

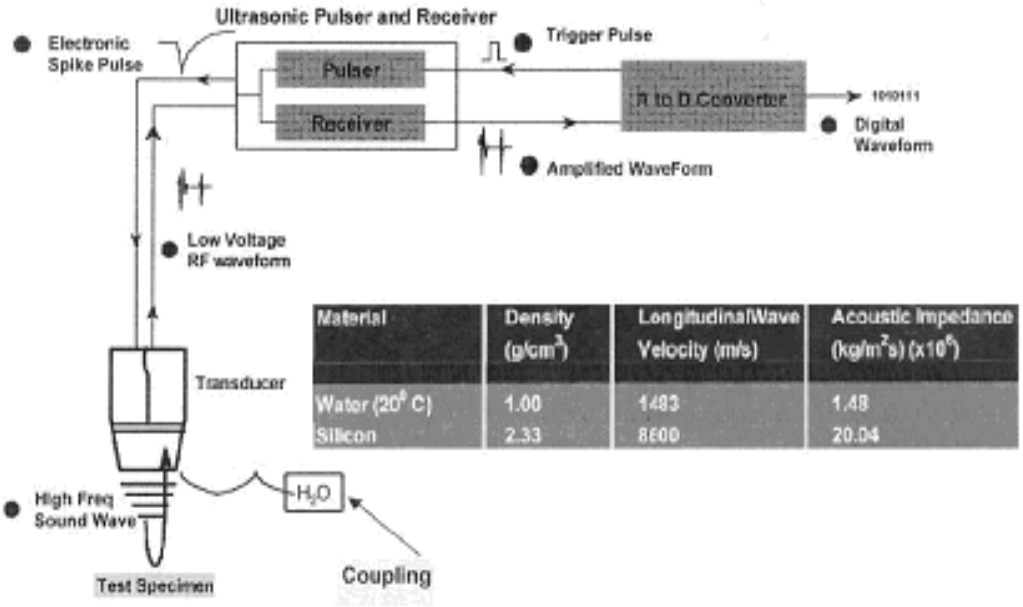

Material	Density (g/cm^3)	Longitudinal Wave Velocity (m/s)	Acoustic Impedance (kg/m^2s) ($x10^6$)
Water (20° C)	1.00	1483	1.48
Silicon	2.33	8600	20.04

Figure 2.2 Principal setup for SAM operation [29]

Chapter 3: Results

3.1 RUV statistics

A crack introduced into Si wafer alters the RUV peak parameters: amplitude, bandwidth and peak position. This is illustrated in Figure 3.1 for two identical 125 mm size Cz-Si wafers. Specifically, the crack in the wafer shows the following features: (1) a frequency shift of the peak position; (2) an increase of the bandwidth, and (3) a reduction of the amplitude. Therefore the RUV approach is essentially based on fast measurement and analyses of a specific resonance peak and rejection of the wafer if peak characteristics deviate from the normal non-cracked wafers.

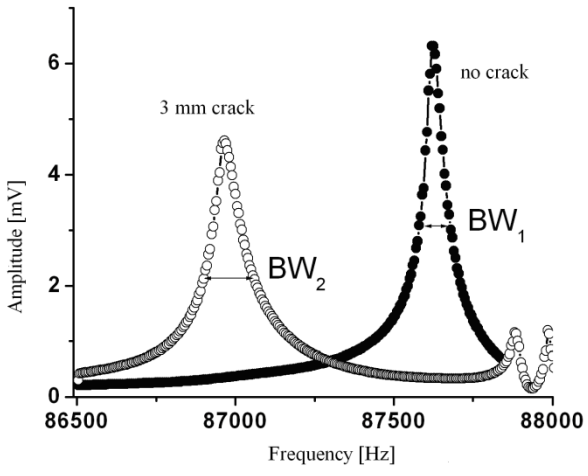

Figure 3.1 Si wafer/cell with crack (open marks) can be separated from a regular wafer/cell (closed marks) using one of three rejection criteria: (1) reduced amplitude, (2) increased bandwidth (BW), and (3) resonance downward frequency shift [31].

One of the technological challenges for using the RUV method as in-line production tool occurred due to the fact that wafers (cells) of even the same size and shape are not identical. They show a statistical variation of the RUV peak characteristics caused by variations of the wafer size, thickness, internal stress, etc. The example of this variation is presented in Figure 3.2 on a set of production-grade as-cut 125 mm cast wafers.

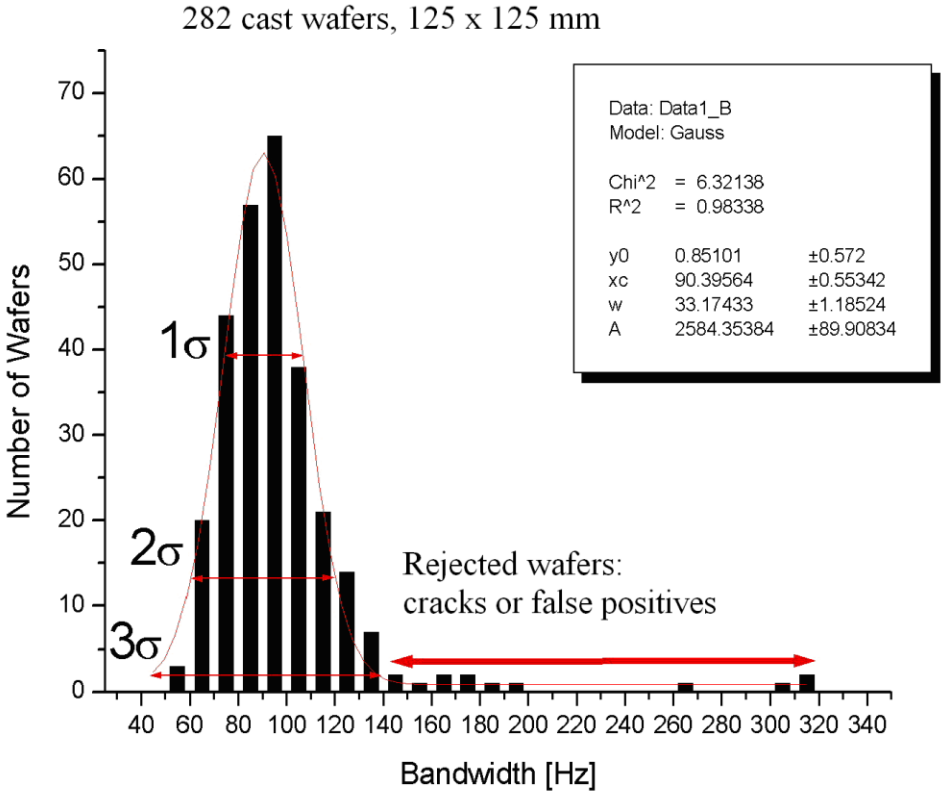

Figure 3.2 Statistics of the bandwidth distribution on a set of as-cut cast wafers. Solid curve is an approximation of the histogram with a normal distribution: mean value = 90.4 Hz, standard deviation = 33 Hz. Wafers with potential cracks are located above the 3σ threshold.

The histogram represents a statistical distribution of the wafer bandwidth (BW) and a fit by a normal distribution with characteristic mean value and a standard deviation (σ). According to one of the crack rejection features the cracked suspects are located above the 3 σ threshold. These suspects, however, can be confused with normal non-cracked wafers, which statistically possess a large BW and may contribute to "false positive" events. The statistical fraction of these false positives is 0.3% for the 3 σ threshold, 5% for the 2 σ threshold and 32% for the 1 σ threshold. To address this issue we suggested using parallel statistical approach applied to all three independent RUV parameters simultaneously. It was assumed that such parallel statistics will dramatically reduce percentage of "false positive" events and increase the accuracy of the RUV method. These experiments were performed on a set of 125 mm and 156 mm Cz-Si solar cells, which show a strong statistical scattering of the RUV parameters. As an example the BW standard deviation was 78 Hz compared to 19 Hz in similar size as-cut Cz-Si wafers.

In a case of screening multiple wafers or cells with identical geometry, a statistical algorithm has been developed and implemented into the RUV system. In this algorithm, the RUV software generates a mean value (M) and standard deviation (σ) for each of the RUV parameters, i.e. amplitude, BW and peak using initial (reference) set of wafers/cells. By this means, 6 statistical parameters of M and σ are calculated. For each RUV parameter the system calculates three thresholds for accept-or-reject command to pass the wafer as a "good" wafer or to reject it as a crack "suspect". The threshold represents a minimum or maximum allowable value of the RUV parameter. In the case of 3σ thresholds, they are defined as $M - 3\sigma/2$ for amplitude and peak position, and

M + 3σ /2 for the BW. In the case of 2σ thresholds, they are M – σ for the amplitude and peak position, and M + σ for the BW (Table 3.1).

Table 3.1 Definition of σ thresholds

	Amplitude	BW	Peak
3 σ case	M – 3 σ /2	M + 3 σ /2	M – 3 σ /2
2 σ case	M – σ	M + σ	M – σ

Additionally, M and σ values are updated along with the RUV measurement, which further improves an accuracy of the threshold calculations. In the experiment we tested both 3σ and 2σ cases. In Figure 3.3 we show a measured RUV parameter on Cz cells. To find wafer with valid statistical deviation we used 3σ rejection threshold in all three parameters.

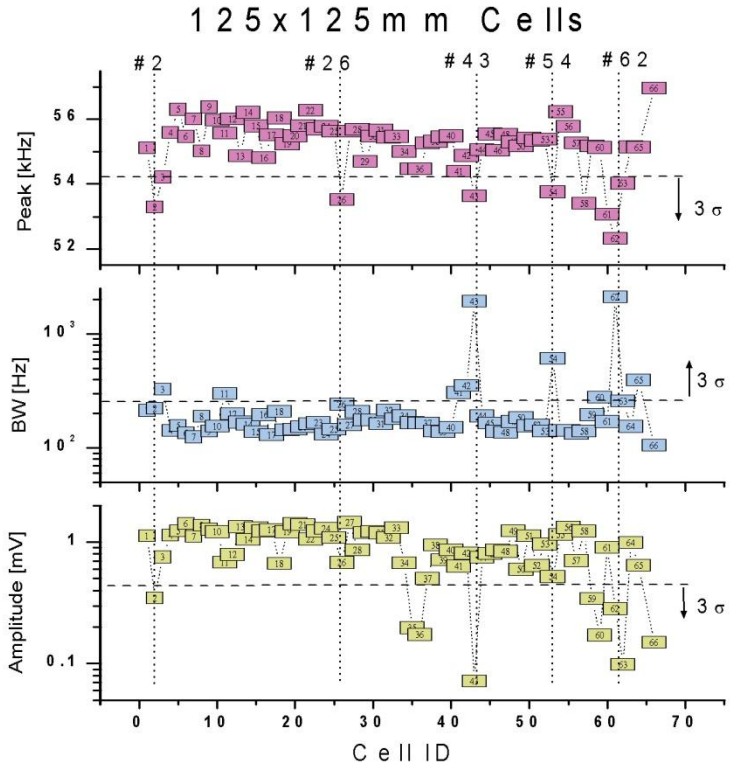

Figure 3.3 RUV statistics of the three parameters of the set of 65 cells. Cells with potential cracks are rejected using 3σ criterion.

We assigned the cell as a cracked "suspect" when at least two of three parameters fell into the 3σ interval. This condition was satisfied in cells with numbers 2, 26, 43, 54 and 62. All suspects were removed from the batch of cells and measured using Scanning Acoustic Microscopy (SAM). SAM mapping provided a clear confirmation of true positive events revealed by the RUV method.

In Table 3.2 we summarize the statistical analyses on 125 mm wafers and cells. Note that percentage of errors which is a total of the "false positives" and "false negatives" is greatly reduced when 3 σ threshold is changed to 2 σ.

Table 3.2 Summary of RUV/SAM comparison on 125 mm x125 mm wafers/cells

Process	**Number of Wafers**	**Number of RUV Rejects**		**Number of True Positives**		**Number of False Positives**	**Number of False Negatives**	
		3 σ	2 σ	3 σ	2 σ		3 σ	**2 σ**
As-cut	112	1	1	1	1	0	0	**0**
Texturing	98	5	5	5	5	0	0	**0**
Diffusion	100	10	10	10	10	0	0	**0**
AR coating	99	3	3	3	3	0	0	**0**
Solar cells	110	8	12	7	11	1	5	**1**
Total	**519**	**27**	**31**	**26**	**30**	**1**	**5**	**1**

Concurrently, the number of "true positive" events when RUV rejects were confirmed by SAM is increased. It has been found that the RUV method provided identification of cells with cracks length down to 3 mm.

Based on this study, we concluded that the RUV method offers a high probability of crack detection with 91% success rate and 9% of errors as a total of false positive and false negative events. We illustrate in Figure 3.4 the results of the statistical analysis on

both sets of 125 mm and 156 mm wafers and cells. Note that this high success rate of the RUV method will lead to a substantial 10-fold reduction in wafers and cells that contain cracks and interfere with production, reducing line throughput and increasing module cost. We propose that different crack rejection coefficients must be incorporated into RUV system software, allowing a production manager to optimize crack inspection depending on the particular technological step of the cell manufacturing.

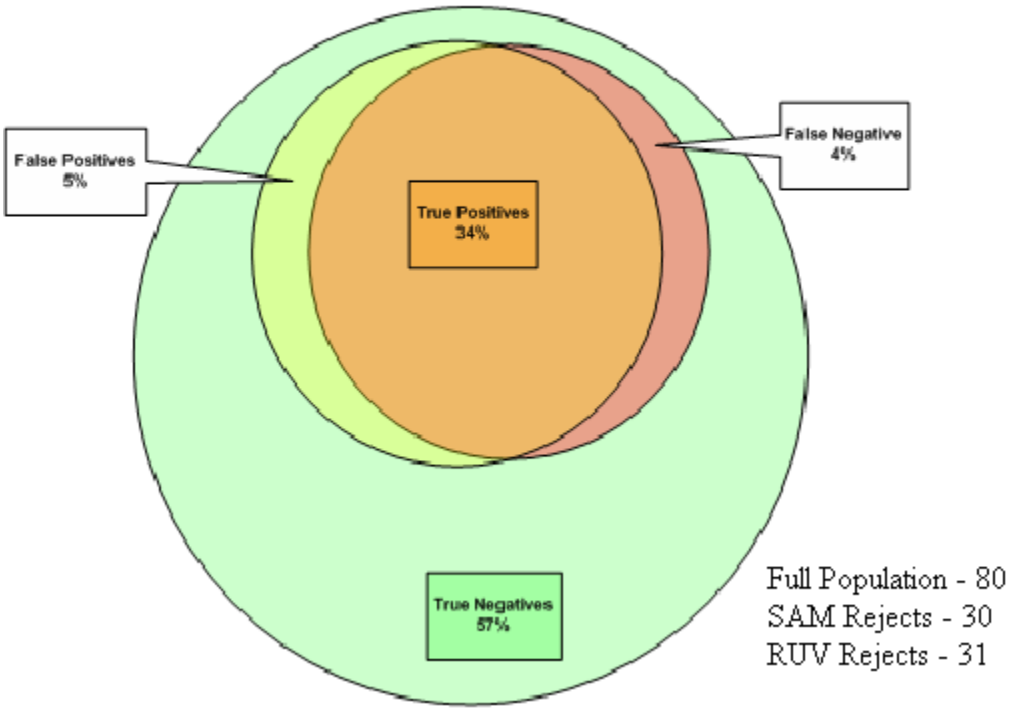

Figure 3.4 Diagram illustrating full statistical evaluation of the Cz-Si wafers and cells.

It was further proposed that the larger deviation of the rejected parameter (e.g. BW) from the mean value or corresponding threshold the larger a damage to the wafer cased by cracks. In Figure 3.5 we present the result of quantitative analyses of the crack

length based on the rejected 125 mm cells. We observed a strong correlation of the BW deviation versus crack length. This experiment demonstrates that the RUV method can be also used for estimation of the wafer damage and therefore serve as a crack characterization technique for in-line application.

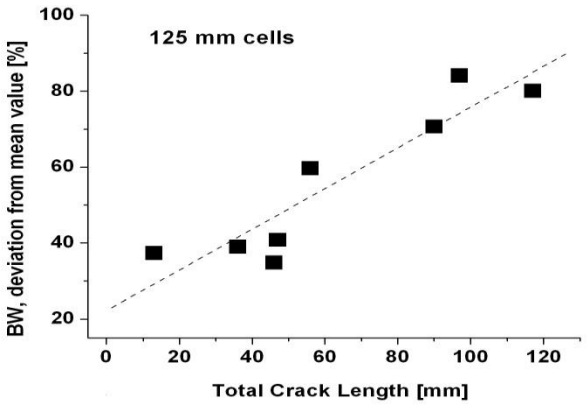

Figure 3.5 Deviation of the RUV peak bandwidth from the mean value versus crack length measured by SAM on a set of 125mm Cz-Si cells.

3.2 Experimental and production grade crack detection

The RUV method relies on a measurement of the resonance ultrasonic vibrations generated in a full-size Si wafer/cell. It includes quantitative analyses of three RUV parameters that characterize the RUV resonance curve - amplitude, bandwidth (BW) and peak position in a frequency scale (peak). Crack is expressed in the RUV method as a reduction of peak amplitude, shift of peak to lower frequency and increase of its BW (Figure 3.6). The hardware details are described earlier.

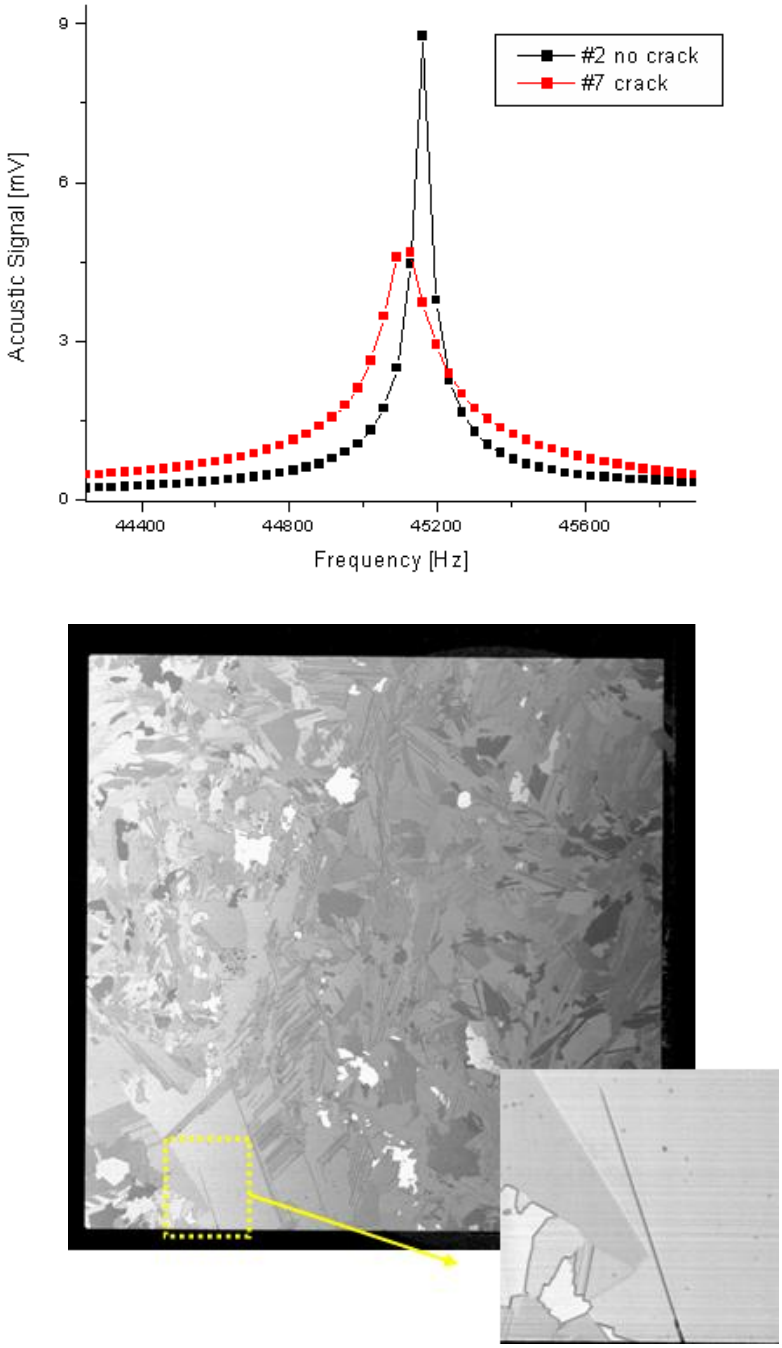

Figure 3.6 RUV parameters shift within in case of cracked wafer and SAM conformation of it. The image size is 158x158 mm, resolution is 100 micron.

In a case of screening multiple wafers or cells with identical geometry, statistical algorithm is developed and implemented in the RUV-2 system. In this algorithm, the RUV software generates a mean value (M) and standard deviation (σ) for each of the RUV parameters, i.e. amplitude, BW and peak as described above.

To reduce the number of false positive events during crack detection, we suggest using a combination of at least two thresholds to identify and reject the wafers with cracks. In this project we tested both 3 σ and 2 σ cases (Figure 3.7).

To prove our assumption two sizes of Cz-Si wafers 125 mm x 125 mm, and 156 mm x 156 mm were used. The wafers were randomly selected at the solar cell producer company Isofoton (Spain) after different process steps from as-cut wafers up to finished solar cells. The RUV system and statistical approach was applied separately to wafers of the same size and the same process step. After the blind test at Isofoton using the RUV system, all rejected wafers and cells were measured using Scanning Acoustic Microscope (SAM) with 100 microns spatial resolution to correlate with RUV data. In some cases to get better confidence of the crack using SAM the local area with crack was remeasured with 10 microns resolution (Figure 3.8). The results of RUV rejection and SAM images are compared.

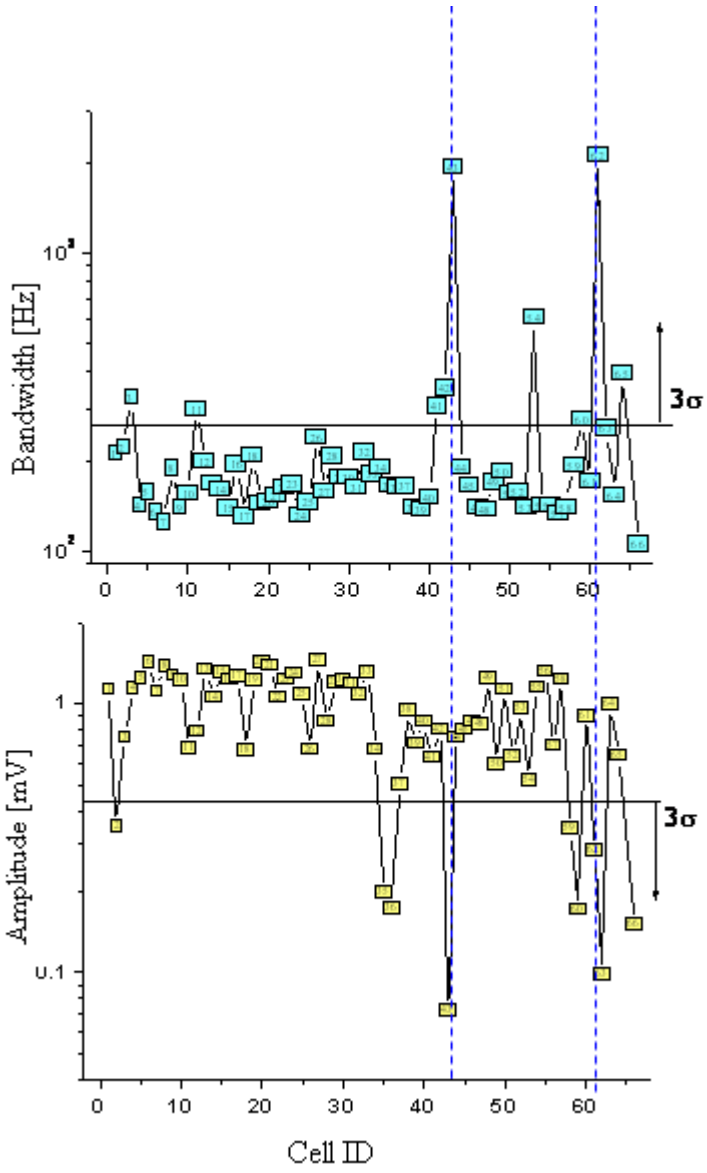

Figure 3.7 RUV of 125mm production-grade Cz-Si cells

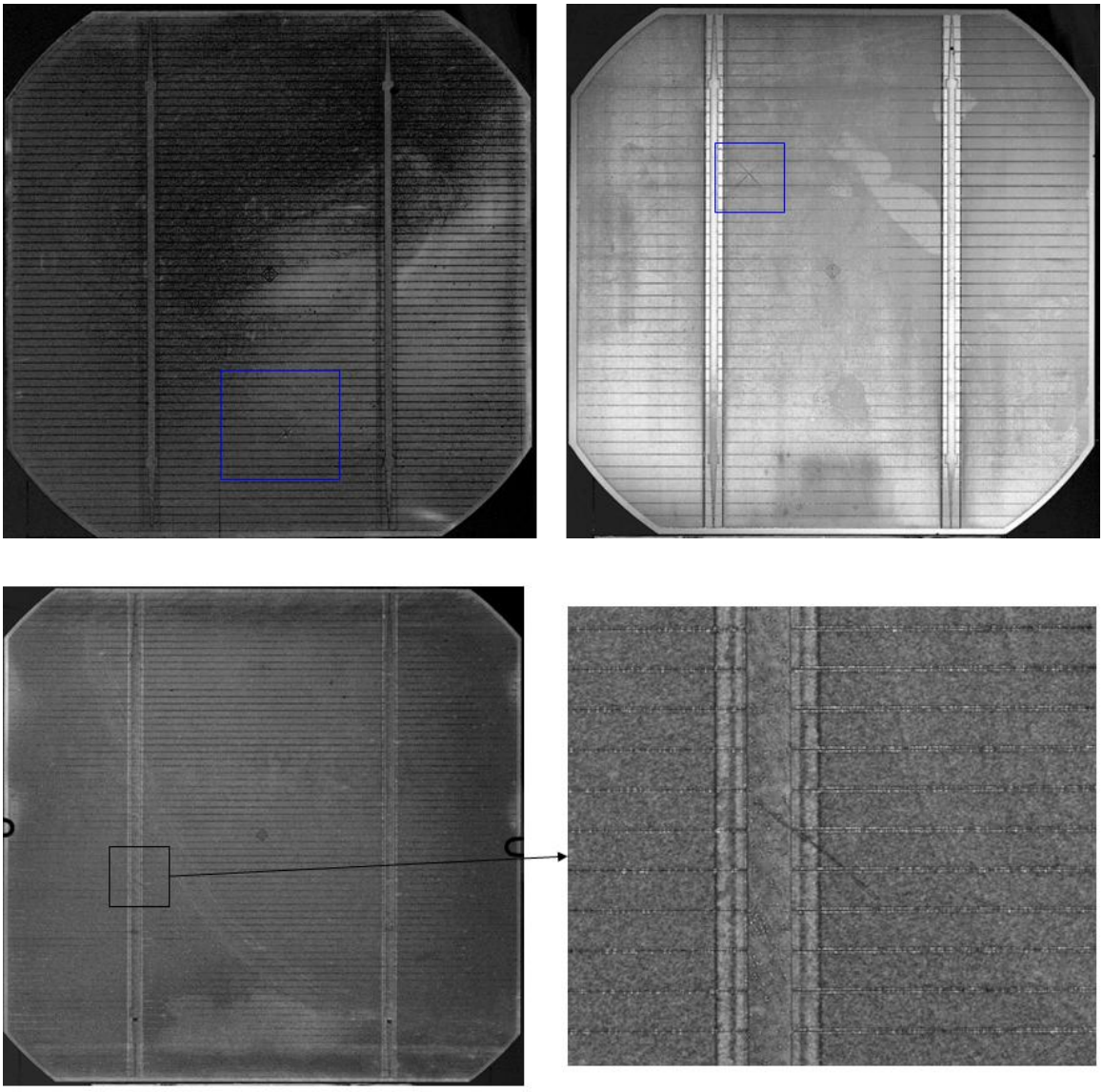

Figure 3.8 SAM images of rejected cells. Image sizes 127 x 127 mm or 158 x 158 mm. Resolution is 100 microns. The last one is 20 x 20 mm, resolution – 10 microns.

Since the characteristic ultrasonic vibration change after each process step, a mean value has to be defined for each step. Therefore, a set of about 100 wafers has been employed for each step to measure the amplitude, bandwidth and frequency of the characteristic peak of the ultrasonic vibration, obtain the mean values and the 3σ thresholds.

In Figure 3.9, the change in mean value, 1 σ threshold and 3 σ thresholds from one process step to the next has been depicted for all parameters. In all cases we can note that the mean values change. The amplitude varies for both sample sizes without any clear trend. The same holds for the bandwidth for the larger sample size. For the 125×125 mm^2 devices, the bandwidth slightly decreases until the final cell step and then increases abruptly. The same trend, but with opposite signs, is observed for the peak frequency for both sample sizes. In all cases, the gap between the mean and threshold widens for solar cells indicating a broadening of the distribution.

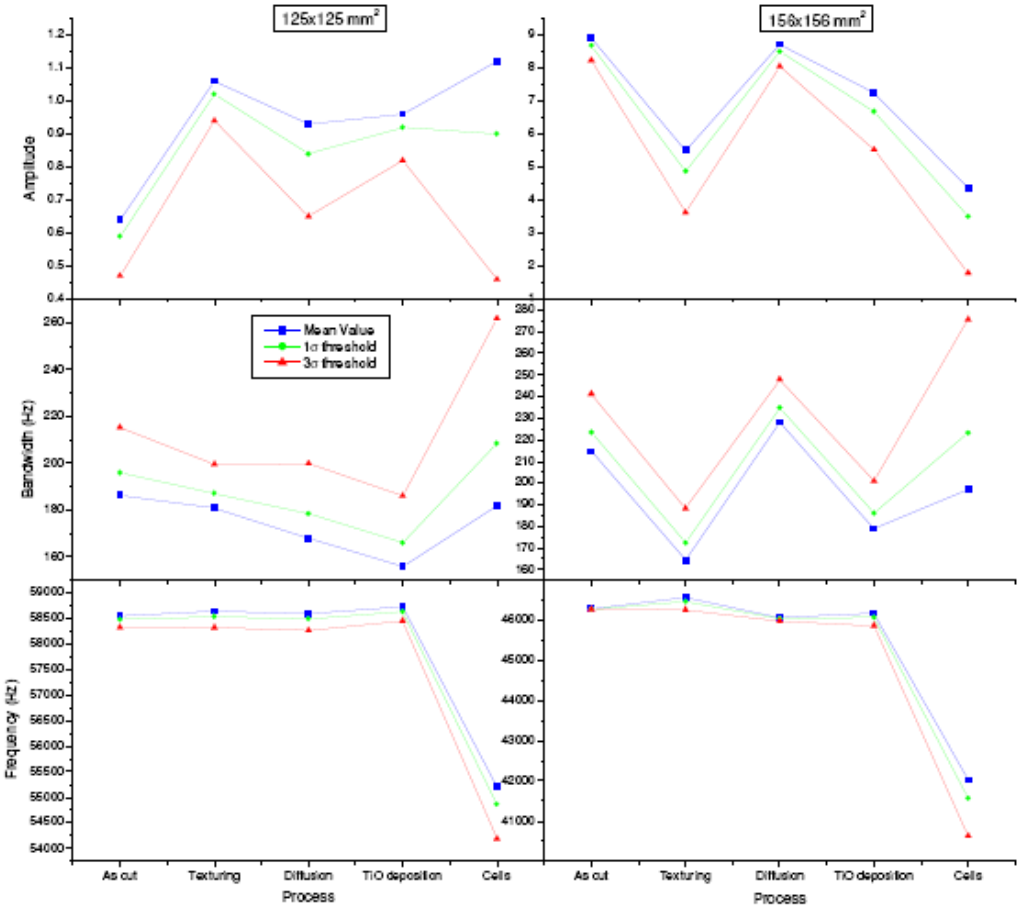

Figure 3.9 Change in mean value, 1σ threshold and 3 σ threshold of amplitude, bandwidth and peak frequency as a function of process step.

This is further highlighted in Figure 3.10, where the distribution of the peak frequency is plotted for as-cut and finished cells of the 125×125 mm^2 group. Note also that the mean value does not coincide with the peak of the distribution if a tail exists at one side of it. This shifts the threshold value towards the tail side if the tail lies on the same side as the threshold. The threshold will shift away from it, if the tail lies on the opposite side as the threshold. A better threshold may be determined by fitting the main peak of the distribution with a normal distribution and using the 3 σ value associated with it.

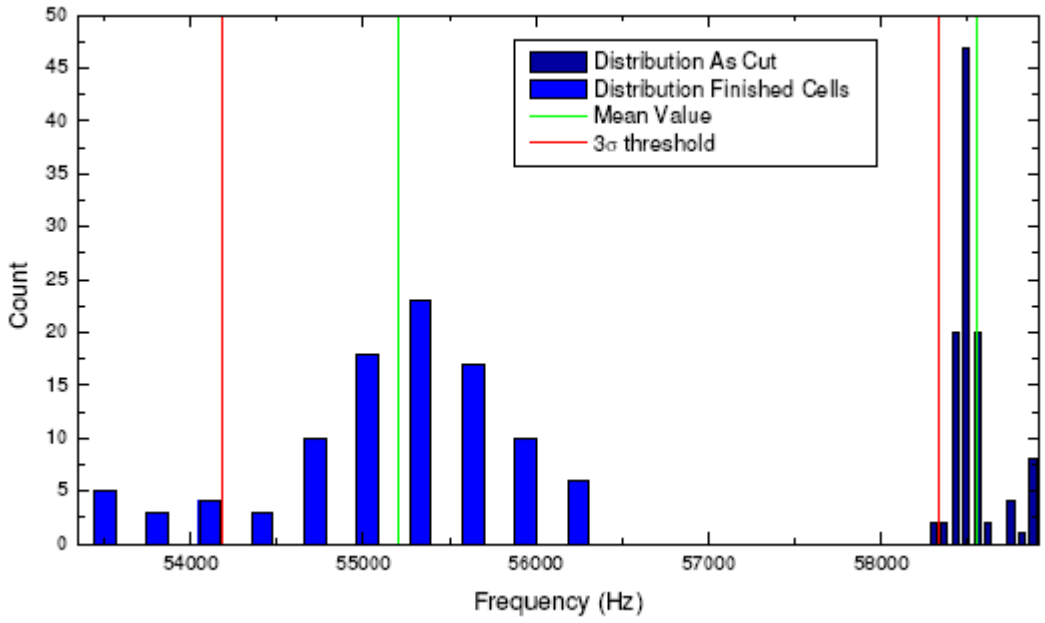

Figure 3.10 Comparison of the frequency distribution of as cut and finished 125×125 mm^2 cells.

The rejection value of the RUV system is based on a statistical deviation from a mean value. Theory and experiments indicate that with increasing crack length, the amount of deviation from the mean value increases. A crack has thus a higher probability

to be detected, if the distribution is narrow. If the distribution of the values is dispersed over a broad range, the 3 σ threshold may overlook cracked cells. The ultrasonic vibration also strongly depends on crystal orientation, which is manifested by a strong change in peak frequency and amplitude. In this case at least 8 of 100 wafers had a different crystallographic orientation tampering the mean value and 3 σ threshold. On the one side this leads to a great number of apparently rejected wafers, on the other side this may push the threshold too far away from the real mean value, effectively excluding a certain number of broken wafers from rejection. The use of wafers of different crystal orientation is, nevertheless, very rare and therefore this extreme case should not emerge in a production environment.

3.3 RUV, PL, SAM comparison

In this section we performed a correlation study of cracks on Si wafers and cells using three independent methods: RUV, SAM, and photoluminescence (PL).

A room temperature PL spectrum in the range of 1050-1580 nm measured on Cz-Si wafers is presented in Figure 3.11a-b. The PL spectrum consists of a single peak with a maximum at ~1125 nm corresponding to the band-to-band transitions in silicon [38]. The spectral position and the shape of this peak are identical in different regions of the wafer, including the area around the crack (Figure 3.11a). Contrary to this, the amplitude of the peak is various across the wafer and also is related to the crack (Figure 3.11b). This will be further shown by the PL mapping technique.

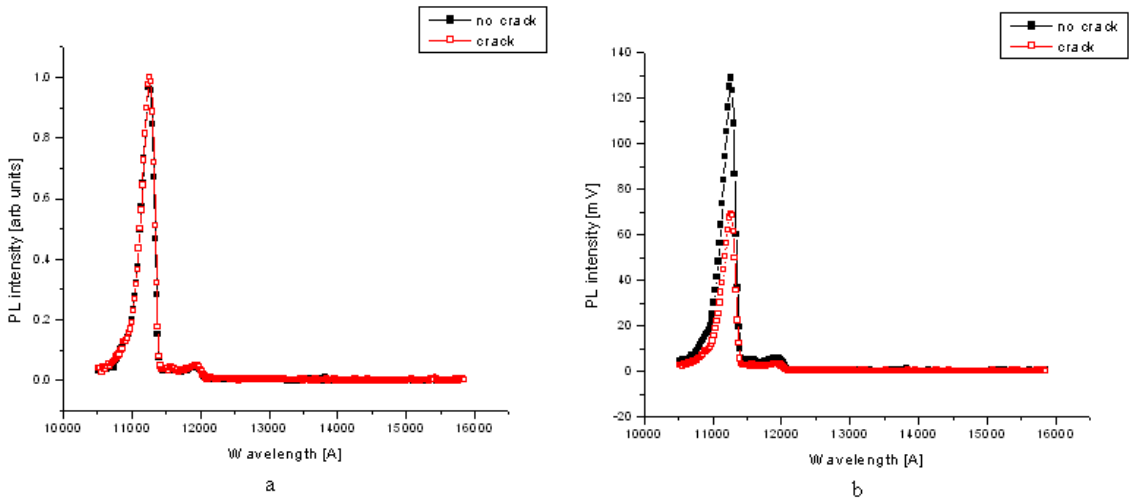

Figure 3.11 a – normalized by intensity PL spectrum measured in the range of 1050 – 1580 nm at room temperature in a single crystal silicon wafer without crack (opened marks) and same wafer in the crack area (closed marks); b – not normalized spectrum in the range of 1050-1580 nm at room temperature without crack (opened marks) and the same sample in the crack area (closed marks)

An illustrative result of the peripheral crack in Cz-Si as-cut wafer measured by the PL mapping and SAM is presented in Figure 3.12a-b. Two images were measured on the same part of a silicon wafer containing ~20 mm crack using PL and SAM. The crack was produced by applying the pressure to the sample edge using the stainless needle. The cracks propagated perpendicular to the sample edge along the <110> cleavage direction. The crack appearance is confirmed by SAM measured with 20 microns resolution on the same sample. Both methods give consistent results in this case. We noticed however, that the PL map in Figure 3.12a contains various artifacts such as reddish area around the crack area which can be attributed to the wafer damage or stress variation caused by a crack. This obviously may complicate crack identification using PL mapping or imaging techniques.

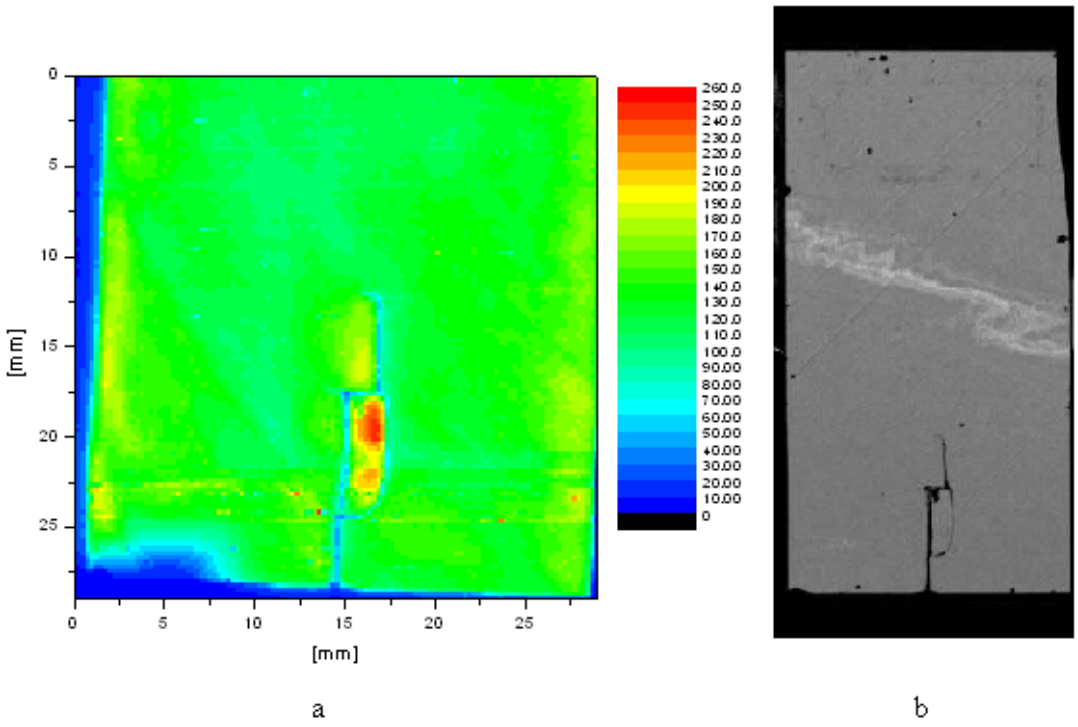

Figure 3.12 a – PL map of crack area 29 x 29 mm at room temperature and 1126 nm wavelength, intensity shown from 0 mV – blue to 260 mV – red; b – SAM image of the same area – 29 x 29 mm, resolution 100 microns.

In Figure 3.13 a-d we are showing PL maps before crack was introduce (a) and actual map of the crack area (b – crack length ~ 17.7 x 24.5 mm) at room temperature and wavelength of 1126 nm. The crack was produced applying the punctual pressure at 45 degrees to the wafer edge. The SAM image measured with 10 microns spatial resolution confirms presence and shape of the crack.

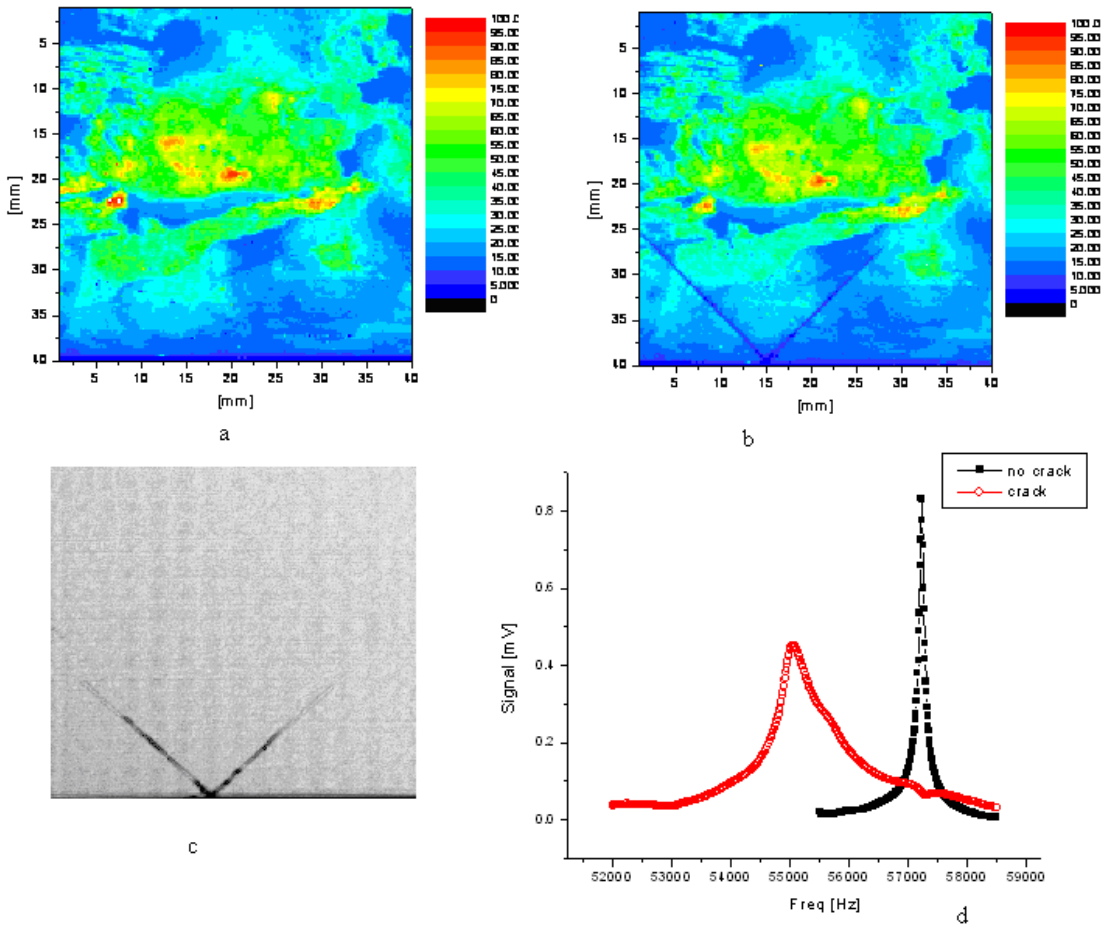

Figure 3.13 a – PL map of area before crack 40 x 40 mm at room temperature and 1126 nm wavelength, intensity shown from 0 mV – blue to 100 mV – red; b – PL map with crack 17.7 x 24.5 mm of the same area; c – SAM image 40 x 40 mm, resolution 10 microns; d – RUV parameters shift on the same wafer before the crack (closed marks) and after the crack (opened marks).

In one of the solar cells using the RUV method we were able to diagnose a partially hidden crack, which was barely seen in the optical technique due to blocking by the busbar (Figure 3.14a-b). Thus RUV method offered a clear advantage in the case of cracks with similar location, which are quite common due to stress applied by contact printing technique.

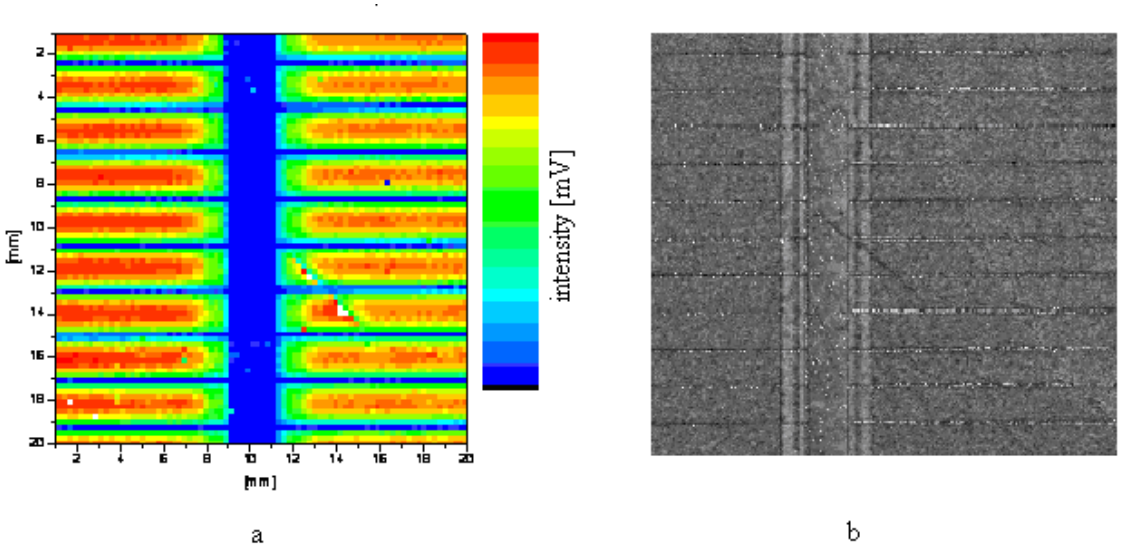

Figure 3.14 a – PL map of crack area 20 x 20 mm at room temperature and 1126 nm wavelength, intensity shown from 0 mV – blue to 40 mV – red; b – SAM image of the same area – 20 x 20 mm, resolution 10 microns.

As a part of Isofoton study we also involve PL mapping as one of the three techniques for identifying the cracks in finished cells. Figure 3.15a-d shows PL maps confirmed also by SAM of cracked area. The crack was introduced by hitting the cell with a diamond pin falling on the cell surface from about 30 mm height. The internal cross cracks with total length of 15 mm were obtained. PL map clearly shows the presence of the crack with reduced PL intensity along the crack lines. We noticed that the crack observed in the PL image is in reality almost double in length compared to the crack in SAM (c and d). This can be explained that in the PL image the real crack length is misinterpreted caused by artificial extension without penetration through the wafer thickness. This will be further demonstrated in scratch experiment below. Interesting observation in the PL mapping technique is that close to the crack area we observed an evident increasing of the PL intensity (shown as red areas along the crack). This effect

could be explained by a local change of the geometry of the cracked surface or alternatively by increased of the local stress around the crack which contributes to the PL intensity. More experiments are necessary to identify the mechanism.

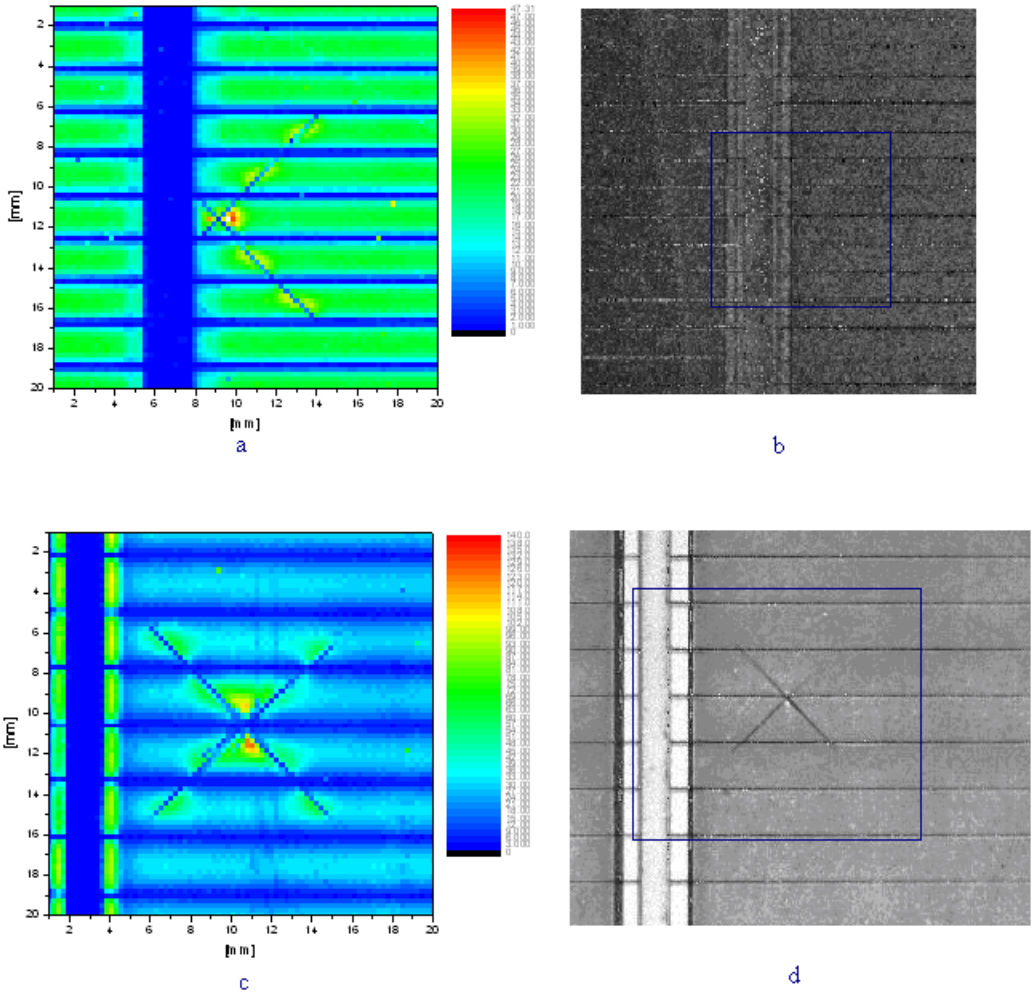

Figure 3.15 a,c – PL maps of crack area 20 x 20 mm at room temperature and 1126 nm wavelength, intensity shown from 0 mV – blue to 140 and 47 mV – red, the actual total crack lengths are ~19 mm and 21 mm; b,d – SAM image of the same area respectively, resolution 100 microns.

In the next experiment we show how the surface scratch could be misinterpreted by the PL method as a crack. Although scratches are one of silicon cell surface defects, they have only a minor impact on the wafer/cell breakage in PV manufacturing. The

scratch was designed by a needle in the direction perpendicular to the wafer edge and tilted at 45 degrees with respect to cleavage direction. This allowed to reliably distinguishing the scratch from the crack. In Figure 3.16a-c we show examples of such a crack. The crack with length approximately 25 mm was introduced by applying the punctual pressure at 45 degrees to the wafer edge. The direction and shape of the crack was confirmed with SAM and PL (Figure 3.16a, b) as well as the wafer was rejected by RUV technique (Figure 3.16c). Thus decreasing of the peak position of no crack versus cracked wafer measurement is 1807 Hz, increasing in BW is 238 Hz and decreasing of amplitude is 2.92 mV. Figure 3.17a-c shows how a scratch defect is revealed by each of three methods on the same silicon wafer. A scratch is clearly visualized in the PL map and has also been found by SAM image measured at the front surface reflection (Figure 3-17a,b). In SAM the wafer was scanned from both sides and analyzed pulses reflected from the front and rear surface of the wafer. This SAM study allowed confirmation that the scratch does not penetrate through the wafer's thickness and is not classified as a crack (Figure 3.17c). In contrast to the PL, there are no changes in the RUV peak parameters caused by the scratch (Figure 3.17d). This experiment justifies high selectivity of the RUV technique to provide diagnostics and characterization of cracks propagated through the wafer thickness.

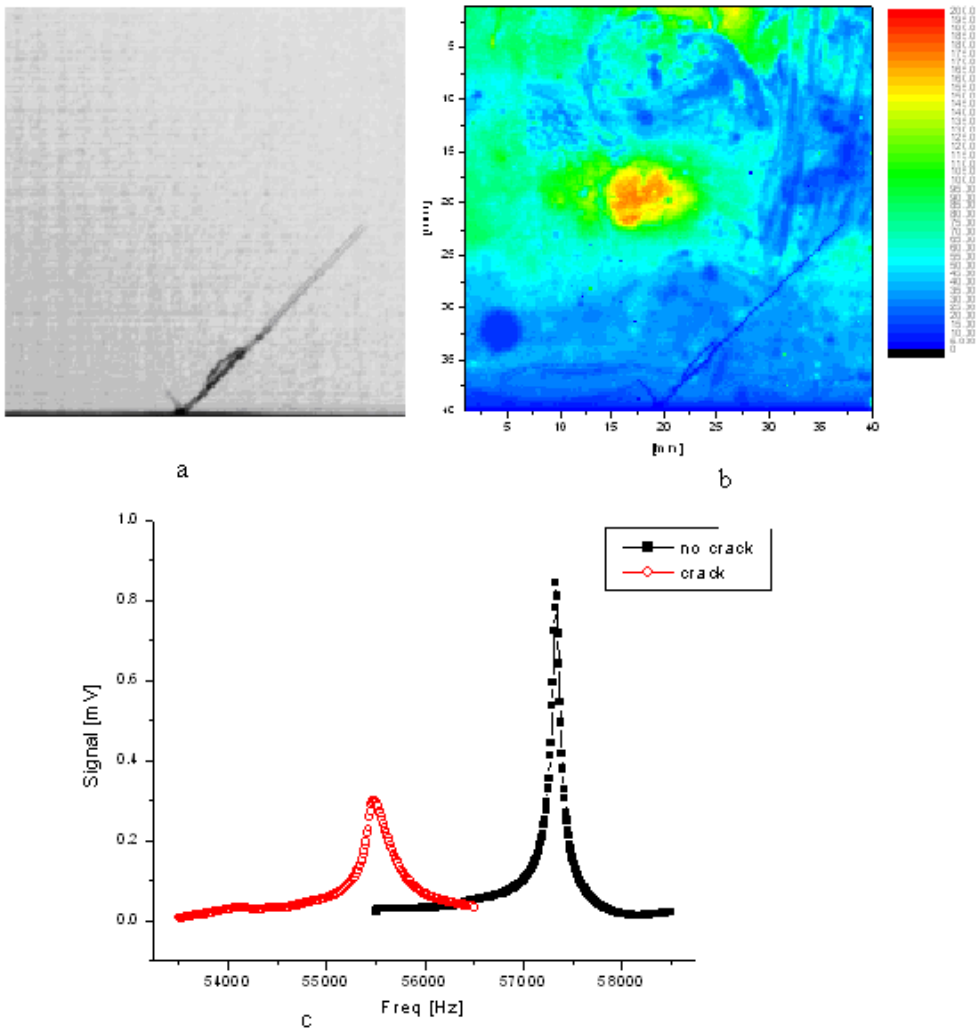

Figure 3.16 a – SAM image 40 x 40 mm wafer area with 25 mm crack; b – PL map of the crack area 40 x 40 mm at room temperature and 1126 nm wavelength, intensity shown from 0 mV – blue to 200 mV – red; c – RUV parameters shift on the same wafer before the crack (closed marks) and after the 25 mm crack (opened marks).

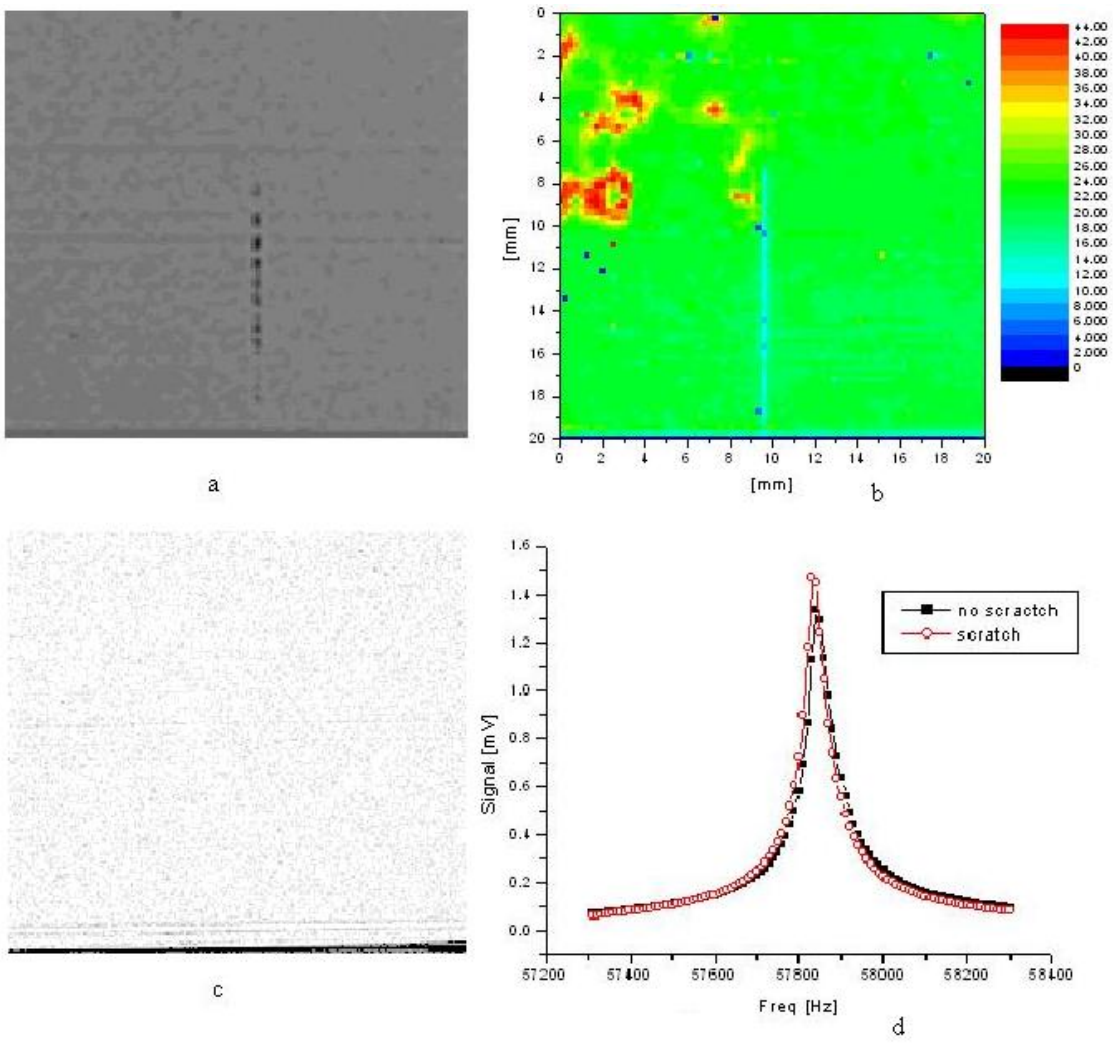

Figure 3.17 a,b – SAM images 20 x 20 mm from the back and front respectively, resolution 10 microns; b – PL map of the scratch area 20 x 20 mm at room temperature and 1126 nm wavelength, intensity shown from 0 mV – blue to 33 mV – red; c – RUV frequency scan on the same wafer before the scratch (closed marks) was introduced and with ~13 mm scratch (opened marks).

Chapter 4: Conclusions and Recommendation

The RUV technique is adapted to fast and non-destructive crack detection in full-size Si wafers for solar cells. The RUV methodology relies on deviation of the resonance frequency vibration curve of the wafer with periphery crack versus non-cracked wafers. It includes quantitative analyses of three RUV parameters that characterize the RUV resonance curve - amplitude, bandwidth and peak position in a frequency scale. Crack is expressed in the RUV method as a reduction of peak amplitude, shift of peak to lower frequency and increase of its BW.

A new statistical approach is developed and tested to reduce a number of false positive events when screening silicon wafers with randomly distributed RUV characteristics. The statistical approach is based on parallel statistics to identify cracks in high-volume production test. In this algorithm, the RUV software generates a mean value (M) and standard deviation (σ) for each of three RUV parameters. By this means, 6 statistical parameters of M and σ are calculated. For each RUV parameter the system using M and σ □values calculates thresholds for accept-or-reject command to pass the wafer as a good wafer or to reject as a crack suspect. The threshold represents a minimum allowable deviation of the RUV parameter from its mean value.

In the case of screening multiple wafers or cells, the statistical algorithm was applied successfully at single crystal silicon wafers and finished cells from the Isofoton

production line. Both sizes of wafers used by Isofoton - 125 mm and 156 mm - were consistently measured. Resonance peaks for RUV are clearly separated from other features in the f-scans. RUV was applied to all wafers starting from as-cut and including finished cells. The effect of statistical distribution of wafers and cells can be minimized using combined statistics of three RUV parameters.

The RUV crack detections were confirmed by SAM mapping with success rate of 95% using 3 σ -threshold. Thus from more than 1000 wafers and cells (125 mm and 156 mm) scanned, 27 were rejected by RUV and confirmed as a cracked with the SAM; 4 wafers/cells were rejected by RUV but there were no cracks in SAM; and 3 wafers/cells were not rejected by RUV but showed the presence of a crack in SAM image.

It has been also experimentally shown that 2 σ rejection is sufficient interval to identify cracks above 3 mm length. Moreover, 1 mm crack length can be accepted as a limit for 2 σ rejection. This can be improved by using 1 σ rejection with potential increase of false positive events. The RUV method can distinctly be used for as-cut and processed wafers including finished solar cells.

The PL and SAM techniques were employed in the current theses to confirm the RUV methodology. A comparison of three independent techniques for crack detection, RUV, SAM and PL, was performed on selected samples. A high accuracy and selectivity of the RUV method to identify mm-size cracks in wafers and cells was confirmed. In contrast to optical inspection techniques it was experimentally shown that RUV method is not sensitive to surface scratches and therefore provides a firm identification of opened cracks which have the highest probability to initiate the wafer and cell breakage.

Future work to improve the RUV system would consist of:

- Exploring applicability of the RUV method for cells sequentially connected in cell strings.
- Performing theoretical analyses of the resonance vibration modes in mechanically connected silicon plates
- Performing experimental justification of the string concept using RUV approach.

References

1. BP's annual Statistical Review of World Energy 2008, www.bp.com

2. Jonathan G. Dorn, Solar Cell Production Jumps 50 percent in 2007 in Earth Policy Institute, 2007

3. Kasap, S.O., Principles of Electronic Materials and Devices. 2nd ed. 2002: McGraw Hill. 68.

4. www1.eere.energy.gov/.../ images/illust_czoch.gif

5. Goetzberger, A., J. Knobloch, and B. Voss, Crystalline Silicon Solar Cells. 1998: John Wiley & Sons, Inc. 136-137.

6. Schmidt, J., A.G. Aberle, and R. Hezel. Investigation of Carrier Lifetime Instabilities in CZ-grown Silicon. in 26th IEEE Photovoltaics Specialists Conference. 1997. Anaheim, CA.

7. Keck, P.H. and M.J.E. Golay, Crystallization of silicon from a floating liquid zone. Phys. Rev., 1953. 89: p. 1297.

8. Shimura, F., Semiconductor SIlicon Crystal Technology. 1989: Academic Press, Inc. 128.

9. www.tf.uni-kiel.de/.../ advanced/t6_1_3.html

10. Kalejs, J.P. An overview of new developments in crystalline silicon ribbon material technology for solar cells. in 3rd World Conference on Photovoltaic Energy Conversion. 2003. Osaka, Japan.

11. Wronski, C.R., et al. Progress in amorphous silicon based solar cell technology. in RIO 02 - World Climate & Energy Event. 2002. Rio de Janeiro, Brazil.

12. Winer, K., Defect formation in a-Si:H. Physical Review B, 1990. 41(17): p. 12150.

13. Staebler, D. and C.R. Wronski, Reversible conductivity changes in discharge-produced amorphous Si. Applied Physics Letters, 1977. 31(4): p. 292.

14. Anderson, T.L., Fracture Mechanics Fundamentals and Applications. 2nd ed. 1995: CRC Press, Inc. 39,282.

15. Perez, R. and P. Gumbsch, Directional anisotropy in the cleavage fracture of silicon. Physical Review Letters, 2000. 84(23): p. 5347-5350.

16. Hauch, J.A., et al., Dynamic fracture in single crystal silicon. Physical Review Letters, 1999. 82(19): p. 3823-3826.

17. Bailey, N.P. and J.P. Sethna, Macroscopic measure of the cohesive length scale: fracture of notected single-crystal silicon. Physical Review B, 2003. 68: p. 205204.

18. O. Breitenstein, J. Rakotaniana, M. Al-Rifai, M. Werner, Prog. Photovolt: Res. Appl., vol. 12, pp. 529-538, 2004.

19. Rueland, E., et al. Optical u-crack Detection in Combination with Stability Testing for in-line Inspection of Wafers and Cells. in Proceedings of 20th EU PVSEC 2005. Barcelona.

20. Rueland, E., et al. u-crack detection and other optical characterisation techniques for in-line inspection of wafers and cells. in 19th European Solar Energy Conference & Exhibition. 2004. Paris, France.

21. Trupke, T., et al., Photoluminescence imaging of silicon wafers. Applied Physics Letters, 2006. 89: p. 044107.

22. Trupke, T., et al. Fast Photoluminescence Imaging of Silicon Wafers. in Proceedings of WCPEC-4 2006. Hawaii.

23. Fuyuki, T., et al., Photographic Surveying of Minority Carrier Diffusion Length in Polycrystalline Silicon Cells by Electroluminescence. Applied Physics Letters, 2005. 84: p. 262108.

24. Lu, J., et al. Investigation of Electrical Activity of Dislocation and Grain Boundary in Polycrystalline Float Zone Silicon. in NCPV and Solar Program Review Meeting. 2003. Denver, Colorado.

25. Rakotoniaina, J.P., et al. Detection of Cracks in Silicon Wafers and Solar Cells by Lock-in Ultrasound Thermography. in Proceedings of PV Solar Conference 2004. Paris.

26. Connor, Z.M., et al., Using scanning acoustic microscopy to study subsurface defects and crack propagation in materials. JOM, 1998. 50(11).

27. Quate, C.F., A. Atalar, and H.K. Wickramasinghe, Acoustic microscopy with mechanical scanning - a review. Proceedings of the IEEE, 1979. 67(8): p. 1092-1114.

28. Wickramasinghe, H.K., Scanning Acoustic Microscopy: A Review. Journal of Microscopy, 1983. 129(1): p. 63-73.

29. SONIX, i., The A,B,C's of Ultrasonics.

30. Hilmersson, C., et al., Crack Detection in single-crystalline silicon wafers using impact testing. Applied Acoustics, 2006.

31. Dallas, W., Resonance Ultrasonic Vibrations for Crack Detection in Silicon Wafers for Solar Cells, Master's Thesis in Electrical Engineering. 2006, University of South Florida: Tampa, FL.

32. Belyaev, A., et al., Crack Detection and Analyses using Resonance Ultrasonic Vibrations in Full-Size Crystalline Silicon Wafers. Applied Physics Letters, 2006. 88: p. 111907.

33. Belyayev, A., Resonance Acoustic Diagnostics in Silicon Wafers, Master's Thesis in Electrical Engineering. 2002, University of South Florida: Tampa, FL.

34. Scofield, J.H., A frequency-domain description of a lock-in amplifier. American Journal of Physics, 1994. 62(2): p. 129-133.

35. Byelyayev, A., Stress diagnostics and crack detection in full-size silicon wafers using resonance ultraonic vibrations, Doctoral Dissertation in Electrical Engineering. 2005, University of South Florida: Tampa, FL.

36. Wasmer, K., et al., Cleavage Fracture of Brittle Semiconductors from the Nanometer to the Centimeter Scale. Advanced Engineering Materials, 2005. 7(5): p. 309-317.

37. Belyaev, A., et al., Resonance ultrasonic vibration diagnostics of elastic stress in full-size silicon wafers. Semiconductor Science and Technology, 2006. 21: p. 254-260.

38. Tarasov, I., et al., Defect monitoring using scanning photoluminescence spectroscopy. Materials Science and Engineering B, 2000. 871: 51-55.

39. W. Dallas, O. Polupan, S. Ostapenko “Resonance ultrasonic vibrations for crack detection in photovoltaic silicon wafers”, Measurements Science and Technology (2007), 18, pp. 852-858.

40. W. Koch, D. Franke, C. Hassler, J. Kalejs, H.-J. Moeller, Bulk Crystal Growth and Wavering for PV: Handbok of photovoltaic Science and Engineering, Ed. By A. Lique et al., Wiley and Sons, 2003.

41. J.P. Kalejs, Silicon Processing for Photovoltaics II, ed. by C.P. Khattak, K.V. Ravi (Elsevier, Amsterdam, 1987), p. 185

42. MODEL SR850 DSP Lock-In Amplifier User Manual. Stanford Research Systems. Revision 1.8 (02/2007)